

Mineral equilibria at high PT-parameters

Ashchepkov I.V. Monomineral universal clinopyroxene and garnet barometers for peridotitic, eclogitic and basaltic systems

V.S. Sobolev Institute of Geology and Mineralogy SB RAS, Novosibirsk

Abstract. Two new versions of the universal clinopyroxene barometer for peridotite pyroxenites and eclogites and garnet barometer for eclogites and peridotites were developed. They were checked using large experimental data sets for eclogitic (~350) and peridotitic systems (>600). The precision of the universal Cpx barometer for peridotites is slightly less but for the eclogites is nearly the same. The calculated the PTXFO2 sections show wide possibilities of these methods for the petrologic reconstructions.

Keywords: Clinopyroxene, barometer, peridotite, eclogite, basalt, kimberlite, garnet.

Citation: Ashchepkov I.V. (2015). Monomineral universal clinopyroxene and garnet barometers for peridotitic, eclogitic and basaltic systems. *Experimental geochemistry*, T. 3. № . pp. X-XX.

http://exp-geochem.ru/JPdf/2015/XX/XXXXXX_en.pdf

The universal single pyroxene barometer [Ashchepkov, 2002; Ashchepkov et al., 2010] working in the broad range of compositions including Cr-diopsides, omphacites and augites was developed on the semi-empirical calibration of the Jadeite-Diopside internal clinopyroxene exchange: $CaMgSi_2O_6 = NaAlSi_2O_6$

Based on cross-correlations with the *Opx* – based [McGregor, 1974] pressure estimates [Ashchepkov, 2002] and further transformations with the separate *KD* (equilibrium constant) and pressure equations for the eclogitic and basaltic systems [Ashchepkov et al., 2010; 2011]. The later versions were calibrated on the large experimental data sets. The obtained $\Delta P = P_{calc} - P_{exp}$ values were studied for the dependence on each component in formula and their simple combinations and corrections were introduced. Instead of the common activities we used the temperature-dependent empirical equation mainly for the position occupied by trivalent elements. The main new amendment is made for the major multiplier replaced by the function dependent from the Al_2O_3 , Na_2O and FeO and $Fe\#$. Finally instead three separate equations for the common peridotites, pyroxenites and eclogites the universal equation was created. It works slightly less precisely for peridotites but even better for eclogites and pyroxenites.

The *KD* is determined as follows: $KD = Na/Al \times Mg/Ca$ [Ashchepkov 2002].

KD was transformed $KD = Na/AlCr \times Mg/Ca$ [Ashchepkov et al., 2010, 2011].

Final pressure equations for the eclogites, peridotites and pyroxenites are as follows:

$$AlCr = (Al-0.01) \times ((T^{\circ}K-600)/700)^{0.75} + Cr \times (T^{\circ}K-100)/1000 + (4 \times Ti - 0.0125)/(T^{\circ}K-801) \times 650 + 0.55 \times ((Fe-0.23) \times (T^{\circ}K-900)/10000 - K);$$

$$P = 0.275 \times (4 + 8.75 \times (Al + 1.25 \times Na + Fe/(Fe+Mg) - 1) \times KD \times T^{\circ}K^{0.75} / (1 + Fe + Fe \times (T^{\circ}K-600)/1000) - \ln(1273/T^{\circ}K)) \times 40 \times (7 \times Na - Al - 15 \times Ti + 10 \times Cr + Mg/4) + 7.5 \times Si - 20 \times (Al \times Na \times Mg/Ca / (Al - 2 \times Ti + 2Na - 2 \times Fe/(Fe+Mg)) + 50 \times (Na + 0.1 \times Al - 2 \times Ti + 0.05 \times Mg - 0.22 \times Ca - 0.7 \times Na) / Ca)$$

New introductions were made also for the garnet barometer (Ashchepkov, 2006). We used the oxides values to avoid the formula calculations. It was created as a sequence of the transformations of the calculated *P* (pressures). Equations of garnet barometer for peridotites use mainly Ca-Cr relations are used [Sobolev et al., 1973].

$$xcm = CaO + MgO; xd = (CaO + MnO + 2 \times FeO)^{0.4};$$

$$xd = (CaO + MnO + 2 \times FeO)^{0.4};$$

$$P = 5.25 \times Cr_2O_3 / xd + 0.02 \times (T^{\circ}K - 273) + 22.5 \times FeO + MgO / 20 + 0.5 \times CaO - TiO_2 - 12 + FeO / 7;$$

$$P = P \times 2.05 + 0.0045 \times P; P = -0.00007 \times P^3 + 0.0057 \times P^2 + 0.87 \times P;$$

$$P = P + 5.5 \times FeO + MgO / FeO; P = P - (4 - Cr_2O_3) \times 0.9 - (TiO_2 - 0.1) \times 10 - (FeO - 7) \times 2$$

The improvements comparing to the previous version (Ashchepkov, 2006).

For peridotites:

$$P = 0.855 \times P + 0.485 / CaO \times T^{\circ}K / 1050 + TiO_2 \times 200;$$

$$P1 = MgO \times Cr_2O_3 \times (T^{\circ}K - 1050) \times FeO / CaO \times TiO_2 / 7000;$$

$$Fe51 = Fe / 2 \times (Fe + Mg) + 0.000045 \times (T^{\circ}K - 790) - 0.0220;$$

$$CrCa = Cr_2O_3 / CaO; P = P - 6 \times CrCa^2 - 12.6 \times CrCa + 25.5 \times TiO_2;$$

$$P = (P - 40) / (T^{\circ}K - 1000) / FeO \times 10 + P;$$

$$P2 = MgO \times Cr_2O_3 \times (T^{\circ}K - 1200) / 120000;$$

$$P = P + P1 \times Fe51 \times 5 + P2 \times (1 - Fe51);$$

Mineral equilibria at high PT-parameters

For eclogites the Na- admixture [Sobolev, Lavrent'ev, 1971] and Ca/(Ca+Mg) [Bobrov et al., 2009] are used:

$$P = 0.815 \times P + 0.45 \text{CaO} \times T^{\circ}\text{K} / 1150 + \text{TiO}_2 \times 200;$$

$$P = (P + \text{Na}_2\text{O} / \text{TiO}_2 \times 8 + \text{CaO}) / \text{MgO} \times 11 \\ \times 1.20 + 5 \times \text{Na}_2\text{O} / \text{CaO} + 7 \times \text{Na}_2\text{O} / \text{FeO} + \text{TiO}_2 / \text{Na}_2\text{O} \times 3 \\ - 100 \times \text{MnO} / \text{Na}_2\text{O} - 80 \times \text{Fe} / (\text{Fe} + \text{Mg});$$

$$P = P - 20 / (85 - P) \times \text{CaO} / \text{MgO}$$

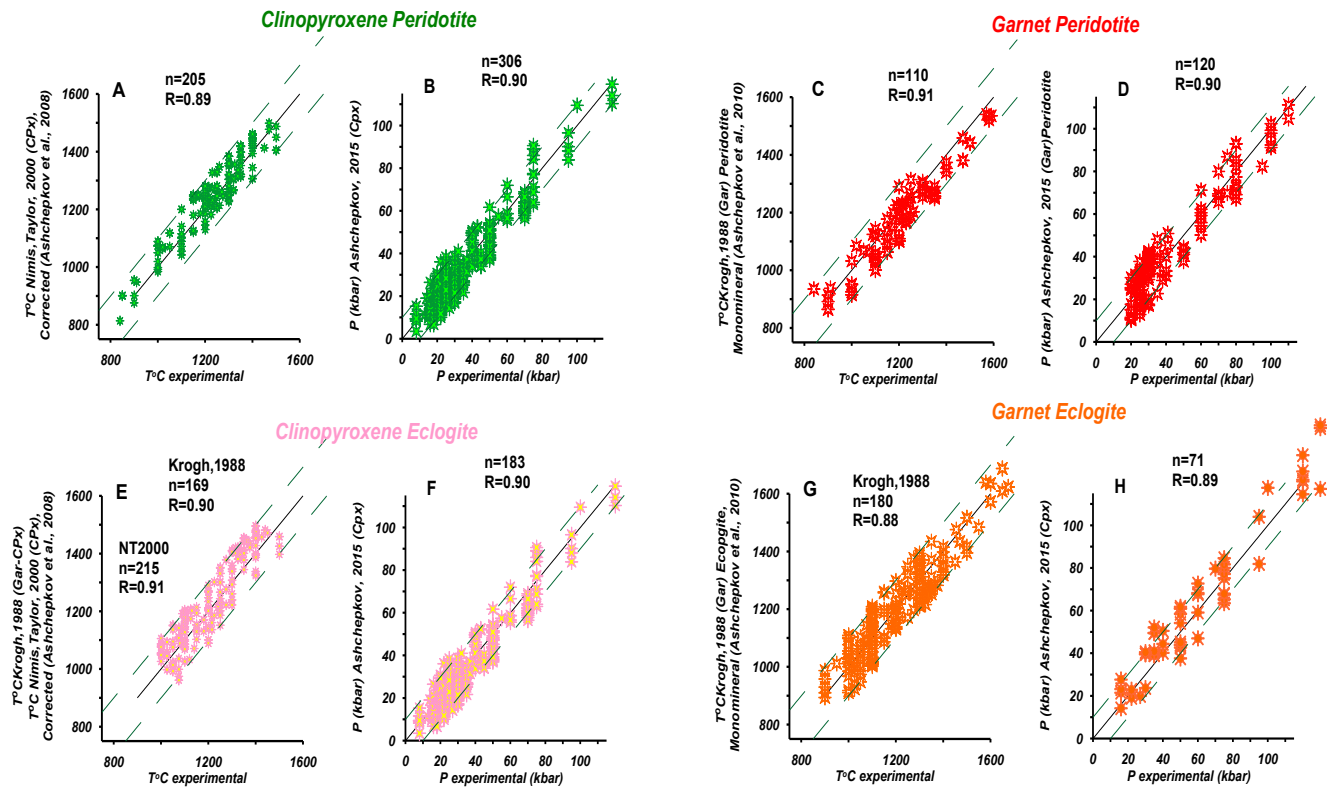


Fig. 1. Correlations of the temperatures and pressures for eclogites using experimental runs:

For peridotites: A – temperatures determined with Gar-Cpx thermometer [Krogh, 1988] and B - pressures with [Ashchepkov et al., 2010 modified]; C – temperatures determined with [Nimis, Taylor, 2000] and D - pressures estimated using garnet barometer [Ashchepkov et al., 2010 modified];

For eclogites: E – temperatures determined with - clinopyroxene thermometer [Nimis, Taylor, 2000] and F - pressures with [Ashchepkov et al., 2010 modified]; G – temperatures determined with [Krogh, 1998] and H - pressures estimated using garnet barometer [Ashchepkov et al., 2010 modified].

The correlations with the experimental data are shown in diagram (Fig.1 D.,H). Temperature are calculating using [Nimis, Taylor, 2000] for clinopyroxenes and [Krogh 1988] in monomineral version [Ashchepkov et al., 2010]. The correlations are shown in diagram (Fig.1: A, E, C, G).

This universal clinopyroxene and garnet thermobarometers for peridotites and eclogite and pyroxenites are using in the Fortran PT program [Ashchepkov, 2011]. They allow calculate simultaneously all PT parameter for all set of mantle xenoliths from the same kimberlite pipe or locality,

Universal equations expands the compositional ranges of minerals for PT reconstructions and gives

more details in mantle sections beneath kimberlite pipes in Siberia and worldwide [Ashchepkov et al., 2010; 2013; 2014] (Fig. 2A, B, C, D). Garnet and clinopyroxene estimates show good mutual good agreements for the same association though many eclogites are not equilibrated.

The reconstructed mantle lithosphere beneath the basaltic volcanoes (Fig.3 A, B) also gives good agreements for the minerals and clinopyroxene thermobarometers allowing the calculations of the PT conditions for pyroxenites and peridotites simultaneously.

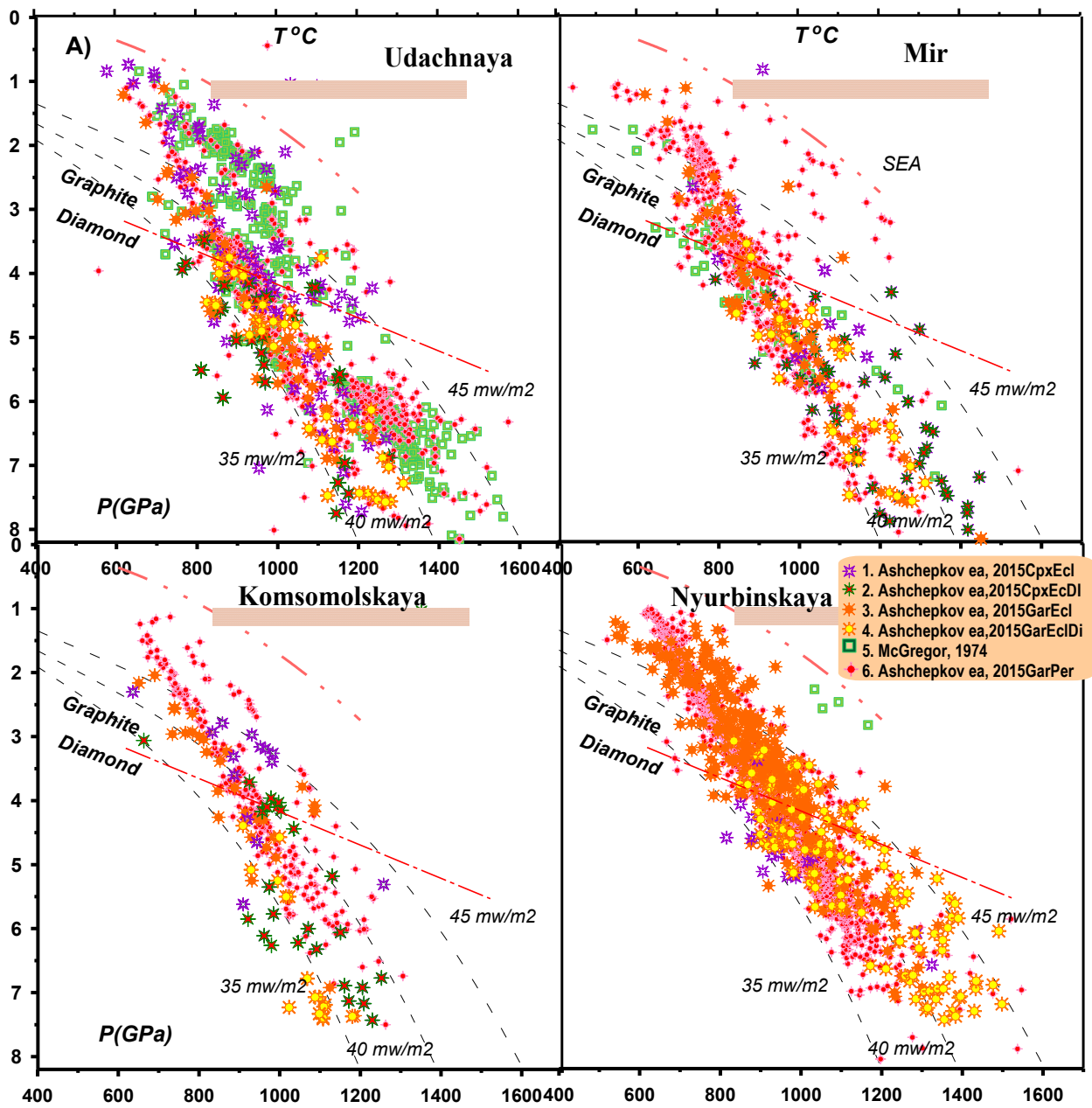
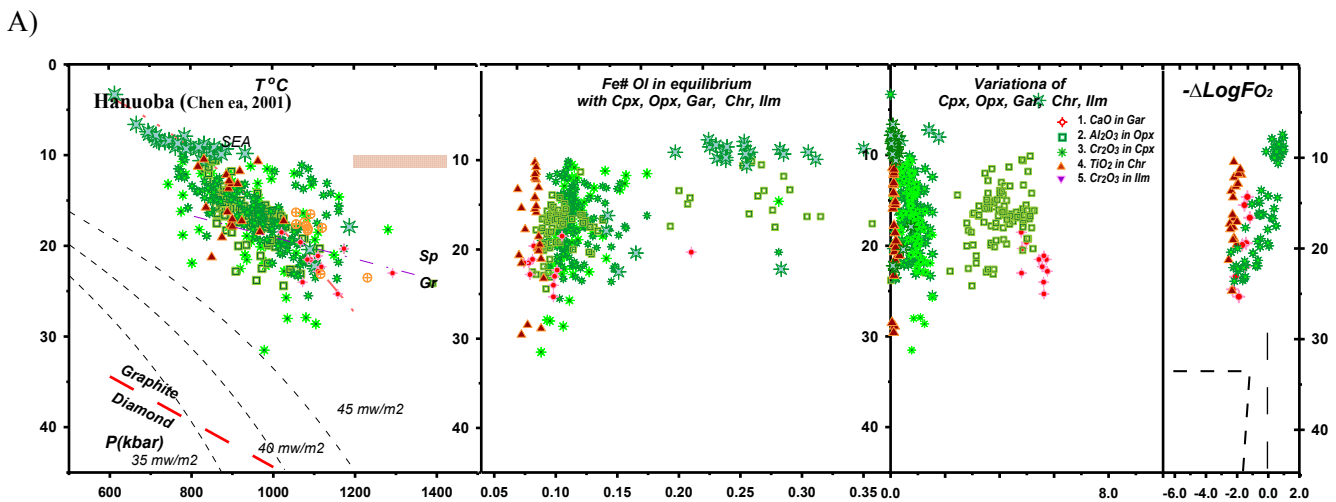


Fig. 2. *PT* diagrams for mantle xenoliths of peridotite and eclogite type together from Udachnaya Mir Komsomolskaya and Nyurbinskaya kimberlite pipes. The signs are shown on the legend.



B)

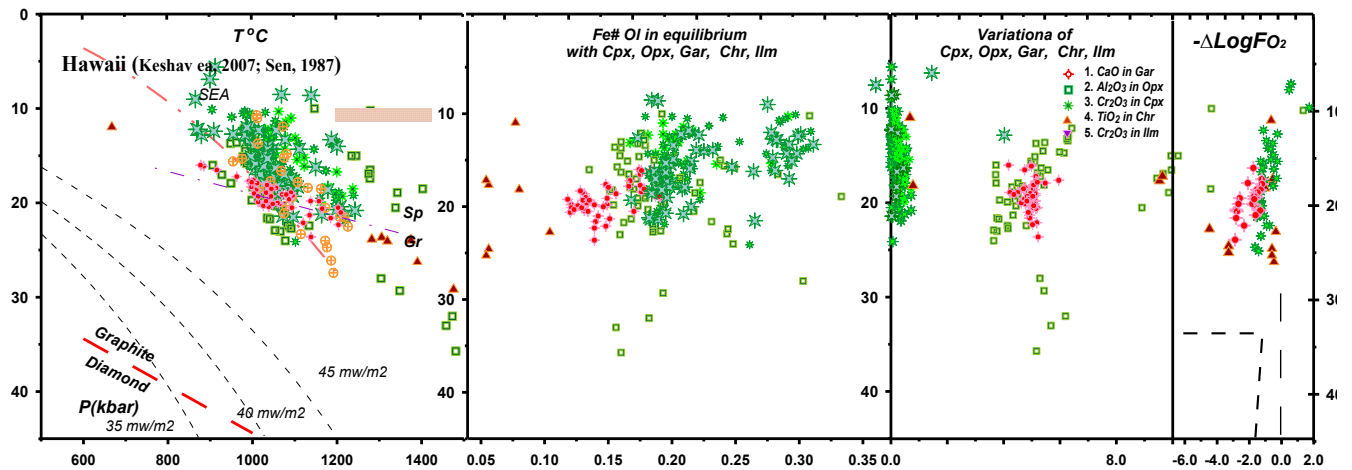


Fig. 3. PTXFO₂ diagrams for the peridotite and pyroxenite xenoliths from the famous localities of mantle xenoliths in alkali basalts A) Hanuoba (China) and B) Hawaii (US).

The work was supported by RBRF grant 11-05-00060a.

References:

- Ashchepkov I.V (2002). Jd-Di barometer for mantle peridotites and eclogites. *Experiment in Geosciences*, Vol.10 N1 pp.137-138.
- Ashchepkov I. V. (2011). Program of the mantle thermometers and barometers: usage for reconstructions and calibration of PT methods. *Vestnik Otdelenia nauk o Zemle RAN*, Vol. 3, NZ6008
- Ashchepkov, I.V., André, L., Downes, H., Belyatsky, B.A. (2011). Pyroxenites and megacrysts from Vitim picrite-basalts (Russia): Polybaric fractionation of rising melts in the mantle? *Journal of Asian Earth Sciences*, Vol. 42, pp.14-37
- Ashchepkov. I.V. (2006). Empirical garnet thermobarometer for mantle peridotites. *Russian Geology and Geophysics*, Vol. 47, 10, pp.1071-1085.
- Ashchepkov, I.V., Pokhilenko, N.P., Vladykin, N.V., Logvinova, A.M., Kostrovitsky, S.I., Afanasiev, V.P., Pokhilenko, L.N., Kuligin, S.S., Malygina, L.V., Alymova, N.V., Khmelnikova, O.S., Palessky, S.V., Nikolaeva, I.V., Karpenko, M.A., Stegnitsky, Y.B. (2010). Structure and evolution of the lithospheric mantle beneath Siberian craton, thermobarometric study. *Tectonophysics*, Vol. 485, pp.17-41.
- Ashchepkov I.V., Vladykin N.V., Ntaflos T., Downes H., Mitchel R., Smelov A.P. Rotman A.Ya., Stegnitsky Yu., Smarov G.P, Makovchuk I. V., Nigmatulina E.N. a, Khmelnikova O.S. (2013). Regularities of the mantle lithosphere structure and formation beneath Siberian craton in comparison with other cratons. *Gondwana Research*, Vol 23, pp. 4-24.
- Ashchepkov, I. V. , Vladykin, N. N., Ntaflos, T., Kostrovitsky, S. I., Prokopiev, S. A., Downes, H., Smelov, A. P., Agashev, A. M., Logvinova, A. M., Kuligin, S. S., Tychkov, N. S., Salikhov, R. F., Stegnitsky, Yu. B., Alymova, N. V., Vavilova, M. A., Minin, V. A., Babushkina, S. A., Ovchinnikov, Yu. I., Karpenko, M. A., Tolstov, A.V., Shmarov G. P. (2014). Layering of the lithospheric mantle beneath the Siberian Craton: Modeling using thermobarometry of mantle xenolith and xenocrysts. *Tectonophysics*, Vol.634, pp.55-75.
- Bobrov, A.V., Dymshits, A.M., Litvin Yu.A. (2009). Conditions of Magmatic Crystallization of Na-bearing Majoritic Garnets in the Earth Mantle: Evidence from Experimental and Natural Data. *Geochemistry International*, Vol.47, pp. 951–965.
- Brey, G.P., Kohler, T. (1990). Geothermobarometry in four-phase lherzolites. II. New thermobarometers, and practical assessment of existing thermobarometers. *Journal of Petrology*, Vol.31, pp.1353-1378
- Chen, S.H., O'Reilly, S.Y., Zhou, X.H., Griffin, W.L., Zhang, G.H., Sun, M., Feng, J.L., Zhang, M., (2001). Thermal and petrological structure of the lithosphere beneath Hannuoba, Sino–Korean craton, China: evidence from xenoliths. *Lithos*, Vol.56, pp.267–301.
- McGregor, I.D. (1974). The system MgO–Al₂O₃–SiO₂: solubility of Al₂O₃ in enstatite for spinel and garnet–spinel compositions. *Am. Mineral.*, Vol.59, pp.110–190.
- Nimis P., Taylor W. (2000). Single clinopyroxene thermobarometry for garnet peridotites. Part I. Calibration and testing of a Cr-in-Cpx barometer and an enstatite-in-Cpx thermometer. *Contributions to Mineralogy and Petrology*, Vol.139, pp.541-554.
- Keshav, S., Sen, G., Presnall, D. C. (2007). Garnet-bearing xenoliths from Salt Lake Crater, Oahu, Hawaii: High-pressure fractional crystallization in the oceanic mantle. *Journal of Petrology*, Vol.48, pp.1681-1724.
- Krogh, E. J. (1988). The garnet-clinopyroxene Fe-Mg geothermometer a reinterpretation of existing experimental data. *Contributions to Mineralogy and Petrology*, Vol.99, pp.44-48.
- Sobolev, N.V., Lavrentev, Y.G., Pokhilenko, N.P., Usova, L.V. (1973). Chrome-Rich Garnets from the Kimberlites of Yakutia and Their Parageneses. *Contributions to Mineralogy and Petrology* 40, 39-52.
- Sobolev, N.V. & Lavrent'ev, Yu.G. (1971): Isomorphic sodium admixture in garnets formed at high pressures. *Contributions to Mineralogy and Petrology*, 31, 1-12.

Kogarko L.N. Experimental constraints on perovskite field stability in larnite-normative high calcium magmas of the kimberlite type

Vernadsky Institute of Geochemistry and Analytical Chemistry of Russian Academy of Sciences

Abstract. Phase melt equilibrium of melilite nephelinites were investigated at 1050-1550°C, 0-35 kbar. Experiments were performed on piston-cylinder high-pressure apparatus. In dry condition the order of crystallization melilite nephelinite: olivine–melilite–pyroxene–nepheline. Addition of 5% CO₂ leads to the formation of perovskite at temperatures 1050-1110°C. The appearance of perovskite in the presence of CO₂ is consistent with geological data, which demonstrated extensive crystallization fields of this mineral in carbonatites and melilitites.

Keywords: phase equilibrium of perovskite in larnite-normative melts. Polar Siberia.

Citation: Kogarko L.N. 2015. Experimental constraints on perovskite field stability in larnite-normative high calcium magmas of the kimberlite type. *Experimental Geochemistry*. T. № X-XX. Cc. X-XX. http://exp-geochem.ru/JPdf/201X/XX/XXXXXX_rus.pdf

Perovskite is a principal concentrator of rare earths, Nb and radioactive elements in larnite-normative alkaline rocks. Therefore, investigation of phase equilibria with perovskite is necessary for our understanding of the formation of mineral deposits of strategic raw material. Present work is aimed at the studying of phase equilibria during the melting of the most enriched in CaO and undersaturated with respect to silica melilite nephelinites, which are widely represented in Polar Siberia and Kola Peninsula.

Experiments were performed on piston-cylinder high-pressure apparatus. Starting material was glass of a given composition prepared from oxides and carbonates (Tab. 1). Certain amounts of starting material were placed into capsules made of graphite or spectral pure iron with the addition of either water or silver oxalate (the source of carbon dioxide). In a case when volatile components were involved capsules made of platinum or silver-palladium were utilized.

Experiments at 5 kbar and oxygen fugacity corresponding to quartz-fayalite-magnetite buffer permitted to establish crystallization order of melilite nephelinite: olivine–melilite – pyroxene – nepheline. Liquidus temperature is 1240°C. Addition of 5% CO₂ leads to the formation of perovskite at temperatures 1050-1110°C. The appearance of perovskite in the presence of CO₂ is consistent with geological data, which demonstrated extensive crystallization fields of this mineral in carbonatites and melilite nephelinites. Experimental data (Brey Green, 1976; Dasgupta et al., 2007) confirm the formation of larnite-normative melilite nephelinites during the partial melting of mantle rocks only under elevated activity of carbon dioxide. Alternative possible reason of perovskite crystallization is significant

increase in TiO₂ activity in the melt in the presence of carbon dioxide (Ryerson, Watson, 1987).

Table 1. Composition of starting material

Component	Melilite nephelinite	Synthesized glass
SiO ₂	39.08	40.33
TiO ₂	2.21	2.28
Al ₂ O ₃	10.03	8.83
Fe ₂ O ₃	4.95	-
FeO	4.53	10.24
MnO	0.17	-
CaO	20.84	21.40
MgO	11.01	10.70
Na ₂ O	3.72	3.20
K ₂ O	2.82	2.02
P ₂ O ₅	0.15	-
etc.	0.84	-
Sum	100.62	99

This work has been supported by the programs of Russian Academy of Sciences.

References:

1. Brey G. & Green D.H. 1975. The role of CO₂ in the genesis of olivine melilitite. *Contributions to Mineralogy and Petrology*. 49, 93-103.
2. Dasgupta R., Hirschmann M. M. & Stalker K. 2006. Immiscible transition from carbonate-rich to silicate-rich melts in the 3 GPa melting interval of eclogite CO₂ and genesis of silica-undersaturated ocean island lavas. *Journal of Petrology*. 47, 647-671.
3. Dasgupta R., Hirschmann M.M. & Smith N.D. 2007. Water follows carbon: CO₂ incites deep silicate melting and dehydration beneath mid-ocean ridges. *Geology*. 35, 135-138.
4. Ryerson F.J., Watson E.B. 1987. Rutile saturation in magmas: implications for Ti-Nb-Ta depletion in island-arc basalts. *Earth and Planet. Sci. Lett.* 86, 225-239.

Litvin¹ Yu.A., Bovkun² A.V., Kuzyura¹ A.V., Spivak¹ A.V., Limanov² E.V., Garanin² V.K. Study of diamondiferous rocks from xenoliths in kimberlites

¹Institute of Experimental Mineralogy RAS, Chernogolovka Moscow district

²M.V. Lomonosov Moscow State University, Department of Geology, Moscow

Abstract. Diamondiferous peridotite-piroxenite and eclogite-grospidite rocks among upper mantle xenoliths in kimberlites have characteristic distinctions from their diamond-free analogues by compositions of rock forming minerals. The metasomatized diamondiferous eclogites are studied, and fragments of solidified diamond-bearing carbonate-silicate parental melts revealed within the veins and cracks over the rock-forming minerals. Based on the mantle-carbonatite conception of diamond genesis, the version that diamondiferous peridotites and eclogites are formed within mantle chambers of variable ultrabasic-basic carbonate-carbon magmas was justified. Host rocks for the chambers were root diamond-free upper mantle peridotites and eclogites, and their xenoliths were caught by kimberlite magmas together with diamondiferous rocks from the chambers.

Key words: diamond-parental melts chambers, diamondiferous xenoliths, diamond-free xenoliths, carbonate-silicate parental media, peridotites, eclogites, ultrabasic-basic evolution of parental melts.

Citation: Litvin, Yu.A., Bovkun, A.V., Kuzyura, A.V., Spivak, A.V., Limanov, E.V., Garanin, V.K. 2015. Study of diamondiferous rocks from xenoliths in kimberlites. *Experimental geochemistry*. T. № . Cc. X-XX.

http://exp-geochem.ru/JPdf/201X/XX/XXXXXX_eng.pdf

Conditions of petrogenesis of diamondiferous peridotites and eclogites within the mantle substance can be relate to key problems of the mantle petrology and genetic mineralogy of diamond, as well as issues of genesis of mineral inclusions in diamonds and intergrowths of diamonds with minerals crystallizing together. It is considered that diamondiferous and diamond-free eclogites have a common origin in accordance with a version of eclogitization of ocean crust in subduction zones [Ringwood, Green, 1966; Green, Ringwood, 1968; Aulbach et al., 2007].

Diamondiferous eclogites are most widespread among diamondiferous xenoliths, a number of their findings is several times more than a number of peridotites containing diamond. Compositions of minerals of diamondiferous peridotites and eclogites are statistically analogues to minerals of peridotite and eclogite parageneses primary included in diamonds. Initial *in situ* positions of diamonds and phases associated with them are retained in diamondiferous rocks in paragenetic diamond-mineral intergrowths and syngenetic inclusions in diamonds. Diamondiferous peridotite-pyroxenite and eclogite-grospidite rocks among upper mantle xenoliths in kimberlites have characteristic distinctions from their diamond-free analogues by compositions of rock forming minerals. It was noted [Sobolev, 1977], that comparative research of diamondiferous rocks and syngenetic inclusions in

diamonds leads to better understanding of conditions of their genesis.

Studies of samples of diamondiferous eclogites-xenoliths from Yakutia kimberlites from the collection of laboratory of diamond deposits (of department of mineralogy of geological faculty of MSU) were carried out during the work. Experiments at high pressures and temperatures (in conditions of thermodynamic stability of diamond) aimed at experimental modeling of formation of diamond associated with minerals of peridotite and eclogite petrogeneses (analogues of diamondiferous rocks), were carried out at Institute of Experimental Mineralogy RAS. Techniques and methodology of physico-chemical experiments at high pressures and temperatures, as well as analytical methods of microprobe analysis and scanning electron microscopy (SEM) for both diamondiferous eclogite rocks and experimental samples, were used.

The goals of the work are: (1) Study of diamondiferous eclogites: textures, structures and composition of minerals by methods of electron microscopy and microprobe analysis; (2) Clearing up formation conditions of the eclogites based on the mantle-carbonatite conception of diamond genesis; (3) Revealing conditions of genesis of metasomatized diamondiferous rocks. We researched sections and polished sections made from diamondiferous metasomatized eclogites by methods of scanning electron microscopy and microprobe as well as Raman-spectroscopy at IEM RAS.

Images (fig. 1a, b) of sections and polished sections, SEM-photographs of the sections (done using electron microscope CamScan M2300 (VEGA TS 5130MM) testify to their sufficiently complicated textures. Results of studies of compositions of rock-forming diamondiferous eclogites are presented in the table. Researches of compositions of mineral phases and textural peculiarities of diamondiferous eclogites testify to volume preservation of grains of rock-forming garnets at presence of narrow kelyphitic rims. Secondary processes altering grains of rock-forming clinopyroxenes are sufficiently developed. Well-preserved grains are also frequent. Intergranular and betweengranular veins, cavities with secondary materials are characterized.

Rock-forming garnets and clinopyroxenes (omphacites) with mirror-smooth surfaces after polishing are homogeneous by composition (the table). Variations of contents of MgO, FeO и CaO in omphacites as well as MgO, FeO, CaO, Na₂O and Al₂O₃ in garnets are revealed in different eclogite samples. For slightly metasomatized zones, a composition of Na₂O in garnets increases from 0.1 – 0.09 to 0.46 – 1.08. Omphacites with the reduced compositions of Na₂O and Al₂O₃ (jadeite component) at increased MgO и CaO contents are marked. Garnets from diamondiferous eclogites are characterized with higher contents of Na₂O (0.10 - 0.22 weight %) [Sobolev, 1977], introduced by impurity Na-majorite component Na₂MgSi₃O₁₂.

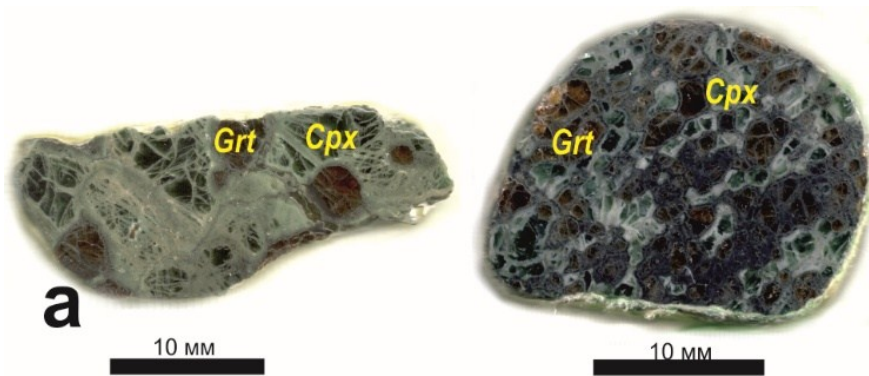


Fig.1. Scanned images (a) and SEM-photographs (b) of samples of diamondiferous eclogites. (Grt – garnet, Cpx – clinopyroxene, carb – carbonate, Djr – djerfisherite, Spl – spinel)

Table. Representative compositions of major rock-forming minerals from samples of diamondiferous eclogites

№ sam.	26		39		40		79		91	
	Grt	Px								
SiO ₂	39.68	54.69	40.97	54.79	38.49	53.87	40.24	54.22	40.24	55.18
TiO ₂	0.76	0.65	0.48	0.29	0.43	0.15	0.18	0.03	0.46	0.45
Al ₂ O ₃	21.26	9.35	19.37	12.33	21.32	8.53	22.39	14.59	22.41	6.62
Cr ₂ O ₃	0.07	0.08	0.12	0.06	0.10	0.14	0.09	0.10	0.00	0.06
FeO	15.72	5.34	12.21	2.74	11.65	2.78	6.75	0.99	14.69	6.20
MnO	0.29	0.02	0.21	0.09	0.30	0.13	0.10	0.04	0.21	0.03
MgO	14.02	9.72	11.70	8.37	9.69	10.20	8.91	7.22	17.42	13.53
CaO	5.76	12.54	12.92	12.77	14.46	16.41	20.65	12.10	3.04	12.23
Na ₂ O	0.17	6.18	0.24	6.82	0.22	4.93	0.08	7.14	0.23	4.70
K ₂ O	0.00	0.09	0.23	0.11	0.05	0.14	0.03	0.14	0.03	0.02
S	0.00	0.00	0.00	0.00	0.00	0.00	0.00	0.07	0.00	0.00
Sum	97.71	98.65	98.44	98.36	96.70	97.28	99.24	96.59	98.73	99.17

Data received by methods of scanning electron microscopy and Raman spectroscopy testify to that there are a lot of pores of irregular shape with sizes up to 50-700 µm, cracks and streaks, which are filled with multiphase substance. Probably, the substance remained from primary diamond-forming parental melts. It is presented by iron-containing magnesite in association with orthopyroxene (Mg,Fe)SiO₃ and kyanite Al₂SiO₅. The associations were found within

grains boundaries of rock-forming minerals and cracks over them. Raman-spectra of experimental samples were recorded in back-scattering geometry using a micro-Raman setup comprised of an Acton SpectraPro-2500i spectrograph and a CCD Pixis2K detector system cooled down to -70°C, as well as microprobe Olympus with the 532 nm line of a YAG CW diode pumped laser at IEM RAS. There are following minerals were identified in them:

Mineral equilibria at high PT-parameters

carbonate, clinoenstatite (Cen), diamond (Diam), orthopyroxene (Opx). There are intensive peaks from monocrystals (carbonate – spectrum 5 and diamond – spectrum 1), as well as less intensive and a little diffuse groups of peaks from fine grained substance of veins (peaks 2-4) in the Raman-spectra (fig. 2).

Spinel $(\text{Fe,Mg})\text{Al}_2\text{O}_4$, orthopyroxene $(\text{Mg,Fe})\text{SiO}_3$, kyanite Al_2SiO_5 , nepheline $(\text{Na,K})\text{AlSiO}_4$, jadeite $(\text{Na,K})\text{AlSi}_2\text{O}_6$, albite $\text{NaAlSi}_3\text{O}_8$, anortite $\text{CaAl}_2\text{Si}_2\text{O}_8$, phlogopite $(\text{K,Na})(\text{Mg,Fe,Ca})_3\text{AlSi}_3\text{O}_{10}(\text{OH})_2$, magnesite

$(\text{Mg,Fe})\text{CO}_3$, calcite (or aragonite) CaCO_3 , Na-carbonate and other alkaline K-Na-Mg-Fe-Ca-carbonates with variable compositions were identified in zones of metasomatically altered minerals, olivine $(\text{Mg,Fe})_2\text{SiO}_4$ was revealed once. Admixture of TiO_2 (up to 0.45 f.u.), sometimes BaO (up to 1.99 f.u.) is characteristic for omphacite. Probably, a major component of metasomatic agent was K-carbonate, simultaneously compounds of Na, Mg, Ca, Ba, Ti and others could be in its composition.

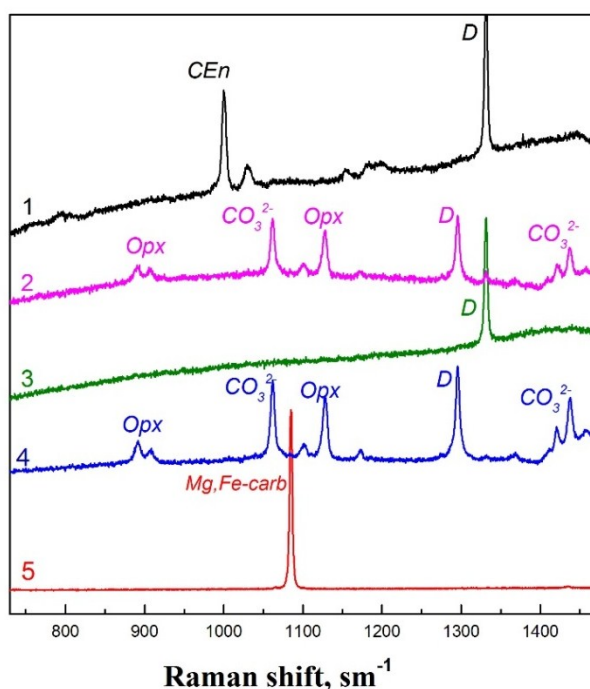


Fig. 2. Raman spectra of substances from cracks and intergranular veins of diamondiferous eclogites. 1 (sample 59) - CEn (clinoenstatite, picks 1000 and 1029 cm^{-1}); D – (monocrystalline diamond, pick 1333 cm^{-1}); 2 (sample 79) – Opx (orthopyroxene, picks 889, 908, 1100, 1129 cm^{-1}); CO_3^{2-} (picks 1102, 1420, 1437, 1458 cm^{-1} of interior vibrations of the anionic group in $(\text{Mg,Fe})\text{CO}_3$; D – (diamond, pick 1295 cm^{-1} , shifted because of little deformations of the crystal); 3 (sample 59) - D – (monocrystalline diamond, pick 1333 cm^{-1}); 4 (sample 59) - Opx (orthopyroxene, picks 889, 908, 1100, 1129 cm^{-1}); CO_3^{2-} (picks 1102, 1420, 1437, 1458 cm^{-1} of interior vibrations of anionic group in $(\text{Mg,Fe})\text{CO}_3$; D – (diamond, pick 1295 cm^{-1} , shifted due to little deformations of the crystal); 5 (sample 40) – Mg,Fe-Carb (pick 1085 cm^{-1} relates to single crystalline $(\text{Mg,Fe})\text{CO}_3$).

Sulfide inclusions, mainly pyrrhotite FeS and nikel pyrrhotite $(\text{Fe,Ni})\text{S}$, pentlandite $(\text{Fe,Ni,Co})_9\text{S}_8$, chalcopyrite CuFeS_2 , and djferfisherite $\text{K}_6(\text{Cu,Fe,Ni})_{23}\text{S}_{26}\text{Cl}$ are presented in the diamondiferous eclogites under study. Interestingly, that djferfisherite, judging by drop-like form of its solidified grain (fig. 1,b), was caught as xenogenic melt immiscible with completely miscible parent eclogite-carbonatite-carbon melt as it is experimentally demonstrated in [Litvin, Butvina, 2004; Litvin et al, 2005; Shushkanova, Litvin, 2007].

Analytical mineralogy of diamondiferous eclogites is studied well enough, it allows to reveal a series of common features. It was reported [Sobolev, 1977; Liu et al, 2008], that diamonds in diamondiferous rocks are mainly arranged between rock-forming minerals with preservation of initial *in situ* contacts. Studies of diamondiferous eclogites using method of high resolution X-ray computed tomography [Taylor et al, 2000] reveal that diamonds are mainly found in interstices clinopyroxene-clinopyroxene and garnet-clinopyroxene. Diamonds as well as garnets are also included in clinopyroxenes. Inclusions of clinopyroxenes in garnets are usual, but diamond inclusions are not characteristic. Sulfide inclusions are irregularly

positioned inside intergranular spaces; they are also reveal themselves as inclusions in garnets, clinopyroxenes, and diamonds. There are distinguished diamonds of 1st earlier generation, that have specific physical and mineralogical peculiarities and, probably, were formed together with rock-forming minerals of diamondiferous rocks [Richardson et al, 1993; Spetsius, Taylor, 2002; Shatsky et al, 2008; Liu et al, 2008; Spetsius et al, 2012]. Intensity of secondary mineralization throw rock-forming minerals of diamondiferous rocks is various. If fracturing is discovered in practically unchanged clinopyroxenes, then a narrow zone of secondary mineralization has revealed along each crack [Taylor et al., 2000].

There are often well-evaluated zones (veins, veinlets, pores) of secondary mineralization over clinopyroxene in contact zones clinopyroxene-clinopyroxene and garnet-clinopyroxene in metasomatized diamondiferous eclogites. Diamonds of 2nd later generation are associated with these zones, that allow to associate their genesis with a period of activation of kimberlitic magmatism. For the period, processes of partial melting of eclogites and secondary metasomatic mineralization are assumed [Spetsius et al., 2012]. It was established

that both earlier and later generations of diamonds in diamondiferous peridotites and eclogites distinguished by contents of admixed nitrogen and extension of its aggregation (more or less than 30%). Diamonds of later generation occur along borders between rock-forming minerals within zones of secondary mineralization, sometimes even in contacts with diamonds of earlier generation [Spetsius et al., 2012].

Chemical and phase compositions of natural parental media for diamonds are directly related to phase relations and compositions of liquid and solid phases of multicomponent multiphase systems. Joint formation of diamonds and paragenetic minerals at the mantle PT-conditions realized in the melts. To reveal chemical composition and phase condition of changeable diamond-forming parental media is unambiguously possible at physico-chemical experimental researches of the systems, which boundary compositions permit to reproduce nature parental medium by major components.

A number of experiments with the use of toroidal high pressure apparatus "anvil-with-hole" was carried out at IEM RAS for researching of syngenetic formation of diamonds and carbonate and silicate minerals of inclusions. A model system peridotite-eclogite-carbonatite-diamond was studied using its inner polythermal section peridotite₃₀carbonatite₇₀ – eclogite₃₅carbonatite₆₅ at PT-conditions of thermodynamic stability of diamond. Starting substances for the experiments were homogeneous mixtures of silicate and carbonate materials prepared in relation with predetermined compositions of the studying systems. Multicomponent (peridotite-carbonatite) – (eclogite-carbonatite) system was studied at 1200-2000°C and 7 GPa (Fig. 3). Peridotite boundary composition corresponds to garnet lherzolite $Per = Ol_{60}Opx_{16}Cpx_{12}Grt_{12}$ (weight %), close to model versions of mineralogical composition of substance of garnet-peridotite facies of the upper mantle [Ringwood, 1975]. Another silicate compound is represented with a model biminerall eclogite $Ecl - Grt_{50}Cpx_{50}$ (weight %) (Sobolev et al, 1972). Multicomponent carbonatite composition K_2O 18.55; Na_2O 1.69; MgO 8.30; CaO 15.08; FeO 15.89; CO_2 40.49 (weight %) reproduce boundary carbonatite composition of the carbonate-silicate substance of primary inclusions in Botswanian natural diamonds [Schrauder, Navon, 1994].

Fig. 3 demonstrates the conditions of complete melting of the system (products of experiments at 1600-1650 °C are represented with homogeneous silicate quenched melt with well-defined dendrite structures). Liquidus phases are Ol, Opx, and Grt, that were detected at temperatures 1700°C, 1600°C, and 1500°C, correspondingly. At temperature decreasing, the following order of crystallization

realizes depending on a melt composition. The Ol-affiliating phases are formed in the sequence: Opx (1600°C), Grt (1550°C), Cpx (1500°C), Ms (1400°C) and multicomponent carbonate (1350°C). The sequences for Opx-affiliating phases: Grt (1500°C), Cpx (1450°C), Ms (1400°C), multicomponent carbonate (1350°C) and for Grt-affiliating phases: Cpx (1500°C), Ms (1350°C) and multicomponent carbonate (1300°C). Subsolidus consists of three phase associations: $Ol+Opx+Grt+Cpx+Ms+Carb^*$, $Opx+Grt+Cpx+Ms+Carb^*$ и $Grt+Cpx+Ms+Carb^*$ (at lower 1370 -1280°C). Magnesite Ms appears first among carbonate solid phases following all other ferrous carbonates of Ca, Na and K. Formation of each individual carbonate phase is accompanied by an additional phase field that makes the phase diagram more complicated. To avoid the complexity, all the carbonate phases are marked with the symbol $Carb^*$. Olivine relates to chrysolite by a composition. It is characterized with lowered and moderate iron indexes. Calcium admixture is also detected in individual cases. Orthopyroxenes are concern to enstatites. There is an admixture of diopside component ($Ca/(Ca+Mg)$ from 0.5 up to 4.0%), as well as Na_2O (up to 0.4 wt.%) in enstatite. Mg index of most of enstatites is within 93-96 %. Orthopyroxene also has a little admixture of Al and K. Clinopyroxene has a moderate iron index, diopside component predominates in its composition. The mineral is notable for increased content of CaO . It relates to diopsides with changeable contents of clinoenstatite, jadeite and chermakite component. Important to point that clinopyroxenes obtained in experiments at any systems composition keep peridotite specialization (excepting of composition $Ecl_{35}Carb_{65}$). Garnet relates to grossular-almandine-pyrope composition. The mineral is characterized with variable iron index and essential portion of calcium component. All garnets are characterized by lowered content of Al and excess of Si. Increased Na-content should be also noted. Garnets as well as clinopyroxenes keep peridotite specialization at each system composition. Carbonates are represented by magnesite, where admixtures of K, Na, Fe, and Al are detected, and by multicomponent carbonate with Al and Na admixtures. An existence of a melt in experimental samples was diagnosed by a presence of characteristic fine-grained quenching aggregate that is represented by carbonates and minerals close to phlogopite. Compositions of melts are changeable due to a variation of the proportion of silicate and carbonate components. Two pseudo-nonvariant peritectic points characterize phase relations of a solidus; reactions of carbonatization of olivine and orthopyroxene are in their base. As a result, three phase associations: $Ol+Opx+Grt+Cpx+Ms+Carb^*$, $Opx+Grt+Cpx+Ms+Carb^*$ и $Grt+Cpx+Ms+Carb^*$ are realized in the subsolidus.

Mineral equilibria at high PT-parameters

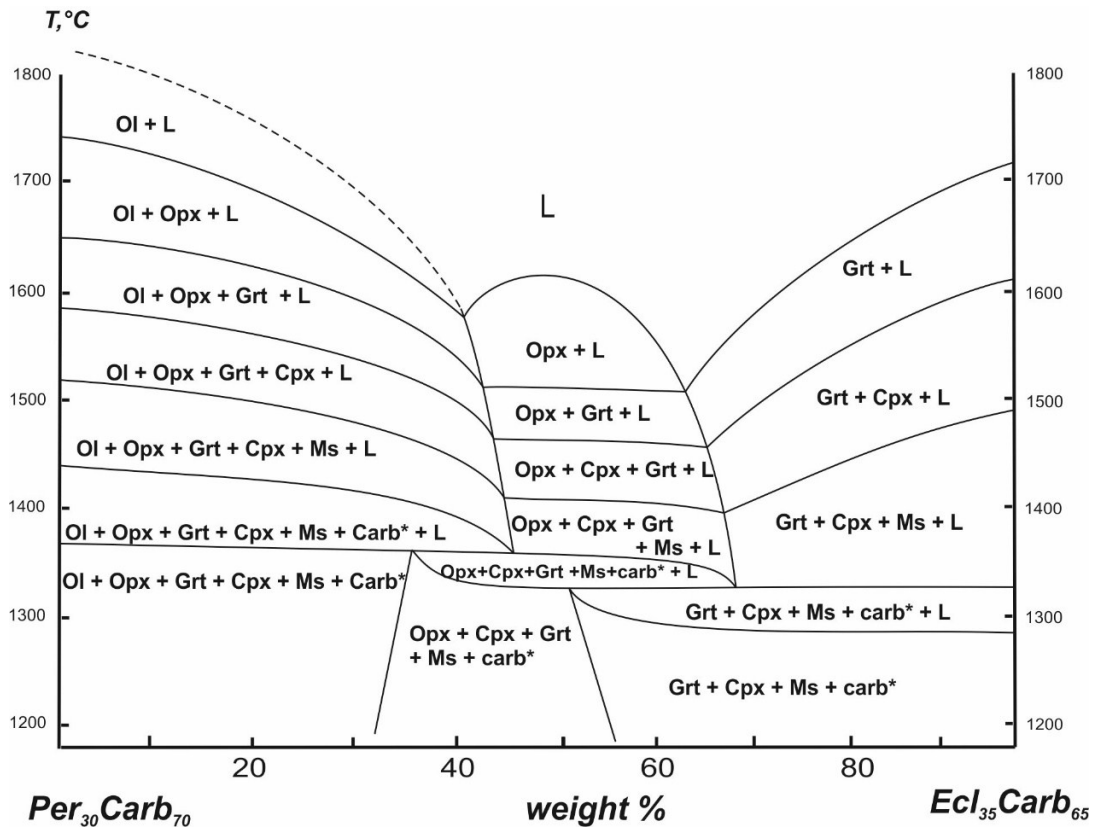


Fig. 3. Phase relations of multicomponent system $Per_{30}Carb_{70}$ - $Ecl_{35}Carb_{65}$ at 7 GPa (equilibrium approximation). Symbols: starting compositions of peridotite – Per, eclogite – Ecl, multicomponent K-Na-Mg-Fe-Ca-carbonate – Carb; Ol – olivine, Opx – orthopyroxene, Cpx – clinopyroxene, Grt – garnet, Ms – magnesite, Carb* - all other carbonates, see text, L – melt.

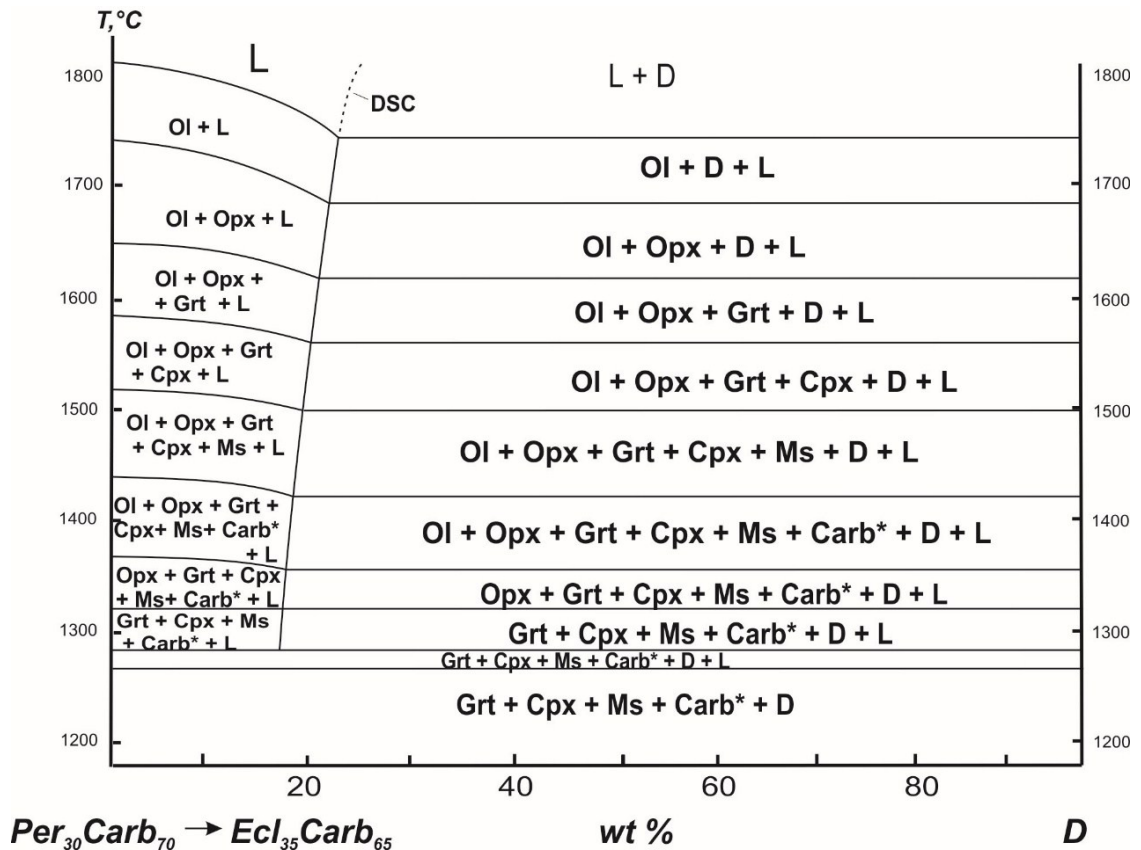


Fig. 4. Schematic “syngensis phase diagram” of multicomponent system $Per_{30}Carb_{70}$ - $Ecl_{35}Carb_{65}$ -D under the regime of fractional crystallization. Symbols: see for Fig. 3; D – diamond, DSC – diamond solubility curve.

Melting phase relations of the system $\text{Per}_{30}\text{Carb}_{70}$ – $\text{Ecl}_{35}\text{Carb}_{65}$ (Fig. 3) are characterized by two pseudo-invariant peritectic points $\text{Ol}+\text{Opx}+\text{Grt}+\text{Cpx}+\text{Ms}+\text{Carb}^*+\text{L}$ and $\text{Opx}+\text{Grt}+\text{Cpx}+\text{Ms}+\text{Carb}^*+\text{L}$ which, probably, demonstrate the reactions of carbonatization of Ol and Opx, correspondingly.

The melting phase diagram of the system $\text{Per}_{30}\text{Carb}_{70}$ – $\text{Ecl}_{35}\text{Carb}_{65}$ at equilibrium approximation demonstrates subsolidus assemblages in the transition stage between the ultrabasic (carbonated peridotite-like assemblage) and basic (carbonated eclogite-like assemblage). The solidus peritectic reactions favour to removal from the subsolidus assemblages ultrabasic phases of a key importance, namely, olivine Ol and orthopyroxene Opx (as the composition of the system moves away from ultrabasic peridotite-like to basic eclogite-like compositions). At the same time for the regime of equilibrium crystallization of primary ultrabasic peridotite-derived melt, the progressive ultrabasic-basic transition of the primary melt composition is impossible. The reason is that the primary composition of the melted and crystallized system is kept constant from start to finish at the regimes of equilibrium melting and crystallization.

The only way in which ultrabasic-basic magmatic evolution of the diamond-parental silicate-carbonate melts has been made possible would be expected under regime of fractional crystallization. Fig. 4 presents the schematic “syngensis phase diagram” demonstrating the sequence of fractional crystallization of ultrabasic diamond-parental peridotite-carbonatite-carbon melt of $\text{Per}_{30}\text{Carb}_{70}$ composition. The diagram is constructed based on the equilibrium phase relations of the system $\text{Per}_{30}\text{Carb}_{70}$ – $\text{Ecl}_{35}\text{Carb}_{65}$ (fig. 3). The boundary symbols ($\text{Per}_{30}\text{Carb}_{70} \rightarrow \text{Ecl}_{35}\text{Carb}_{65}$) in the Fig. 4 make it apparent the starting parental melt composition $\text{Per}_{30}\text{Carb}_{70}$ and the final one $\text{Ecl}_{35}\text{Carb}_{65}$, the boundary symbol D is for carbon (diamond). Starting complete Ol-normative ultrabasic melt the system has the boundary composition $\text{Per}_{30}\text{Carb}_{70}$, and the sequence of the melt crystallization is taken from the diagram on Fig. 3.

The “syngensis phase diagram” of the system ($\text{Per}_{30}\text{Carb}_{70} \rightarrow \text{Ecl}_{35}\text{Carb}_{65}$) – D (Fig. 4) reveals the physico-chemical mechanisms of diamond nucleation and mass crystallization due to its important topological element - diamond solubility curve (DSC). The DSC divides the melting relations diagram into the field of silicate-carbonate melts unsaturated with carbon (on the left) and saturated ones (on the right). The parental melts are completely prepared for diamond formation if a figurative point of composition and temperature of the system is in line with the DSC. Oversaturation of the parental

silicate-carbonatitic melt-solution saturated with dissolved carbon is provided with temperature lowering. At critical oversaturation nucleation and mass crystallization of diamonds proceed simultaneously with formation of paragenetic silicate and carbonate minerals. Melting relations of the system combined with the regime of fractional crystallization control the regularities of sequential formation of diamond-bearing peridotitic and eclogitic rocks as well as trapping by growing diamonds of primary inclusions as peridotitic so eclogitic parageneses.

Study of genesis of diamondiferous peridotites, piroxenites and eclogites, especially their metasomatized species, is possible in the context of a common picture of diamond formation within the substance of the upper mantle and formation of diamondiferous kimberlite pipes within the crust. The main stages are: (1) formation of separate upper-mantle chambers of diamond-forming ultrabasic silicate-carbonate-carbon parental magmas, besides, primary actions should be metasomatic carbonatization of mantle peridotite [Litvin, 1998] and formation of completely miscible carbonate-silicate melts with dissolved carbon in them; (2) physic cooling of the chambers is accompanied with nucleation and crystallization of diamonds paragenetically with peridotite and eclogite minerals in ultrabasic parental magmas in a regime of fractional crystallization (with fragmental capture of paragenetic and xenogenetic minerals and melts by diamonds and formation of diamondiferous peridotites and piroxenites); (3) continuation of the fractional crystallization of parental melts changes their ultrabasic compositions to basic (it is due to the mechanism of “peridotite-eclogite paragenetic conversion [Litvin, 2012]); correspondingly, continuation of diamond crystallization in paragenesis with eclogitic minerals (with fragmental capture of paragenetic and xenogenetic phases by diamonds and formation of diamondiferous eclogites); it should be noted that a duration of formation of diamonds is commensurate with a duration of existence of the mantle chamber of parental magmas with final hardening of solidus melts; (4) through geologically essential time periods – destroying of consolidated chambers by rising flows of kimberlitic magmas, capture of heterogenic material of both the chambers themselves and host differentiated upper mantle rocks and transport of them to the crust, where the kimberlite flows stop and consolidate in temporary cumulative centers; (5) at cooling of the centers the kimberlite magmas continuously solidify releasing fluids dissolved in them with accumulation of gas phase that finally put in force explosive breakouts and moving of a content of the cumulative centers to the earth's surface that ends with a formation of kimberlite pipes.

Support: grant of RFBR 13-05-00835.

References:

1. Ringwood A.E., Green D. 1966. *Tectonophysics*. № 3. Pp. 383-427;
5. Green T.H. and Ringwood A.E. 1968. *Contributions to Mineralogy and Petrology*. V. 18. Pp. 105-16;
6. Aulbach S., Pearson N.J., O'Reilly S.Y., Doyle B.J. 2007. *Journal of Petrology*. V. 48. Pp. 1843-1873;
7. Sobolev N.V. Deep-seated Inclusions in Kimberlites and the Problem of Upper Mantle Composition. Washington, D.C., AGU, 1977. 279 p;
8. Litvin Yu.A., Butvina V.G. 2004. *Petrology*. T. 12. № 4 C. 377-382 ;
9. Litvin Yu.A., Shushkanova A.V., Zharikov V.A. 2005. *Doklady Earth Sciences*. T. 403. № 5. C. 719-722 ;
10. Shushkanova A.V., Litvin Yu.A. 2008. *Canadian Mineralogist*. V. 46. Pp. 991—1005;
11. Liu Ya., Taylor L.A., Sarbadhikari A.B., et al. 2009. *Lithos*. V. 112. Pp. 1014 – 1024. Doi:10.1016/j.lithos,2009.06.036;
12. Taylor L.A., Kelle R.A., Shyder G.A., Wanc W., Carlson W.D., Hauri E.H., McCandless T., Kim K.-R., Sobolev N.V., Bezborodov S.M. 2000. *International Geology Review*. V. 42. Pp. 959-983;
13. Richardson S.H., Harris J.W., Gurney J.J. 1993. *Nature*. V. 366. Pp. 256-258;
14. Spetsius Z.V. Taylor L.A. 2002. *International Geology Review*. V. 44. Pp. 973-987;
15. Shatsky V.S., Ragozin A.L., Zedgenizov D.A., Mityukhin S.I. 2008. *Lithos*. V. 105. Pp. 289—300;
16. Spetsius Z.V., Kovalchuk O.E., Bogush I.N. 2012. In: *Extended Abstracts 10th International Kimberlite Conference*, Bangalore. 101KC-51;
17. Ringwood A.E. 1975. *Composition and petrology of the Earth's mantle*. New York – Toronto, McGraw-Hill. 618 p.;
18. Sobolev V.S., Sobolev N.V., Lavrent'ev Yu.G. 1972. *Doklady Acad. Nauk SSSR*. V. 207. № 1. Pp. 164-167 (in Russian) ;
19. Shrauder M., Navon O. 1994. *Geochim. Cosmochim. Acta*. V. 58. № 2. Pp. 761–771;
20. Litvin Yu.A. 1998. *Russian Geology and Geophysics*. V. 39. № 12, Pp. 1761-1767;
21. Litvin Yu.A. 2012. In *RMS Annual Session combined with the Fedorov Session 2012 "Mineralogy in a whole space of the word"*. Conference proceedings, Saint-Petersberg

Gorbachev¹ N.S., Ravna² E., Kostyuk A.V., Nekrasov¹ A.N., Kullerud² K. Phase relationship and geochemistry of garnet-bearing carbonatites of Trosø area, Norway

¹Institute of Experimental Mineralogy RAS, Chernogolovka Moscow district

²University Tromsø, Norway

Abstract. The phase composition and geochemistry of garnet-containing carbonatites UHPC Tromsø area studied. The matrix of UHPC calcite-dolomite composition contains inclusions of garnet, and accessory minerals - apatite, sphene, ilmenite, rutile. There

are three generation of garnet: Grt1, depleted in REE (<2.10⁻² wt.%); Grt2-3, anomalously enriched (up to 4-8 wt.%) in LREE. Carbonate Cb and silicate Si components of UHPC differ on concentration of trace elements. Anomalous REE distribution in UHPC indicates a lack of equilibrium between Grt and carbonatite melt.

Keywords: carbonatite, high pressures, phase composition, geochemistry, experiment.

Citation: Gorbachev N.S., E. Ravna, A.V. Kostyuk, A.N. Nekrasov., K. Kullerud (2015) Phase relationship and geochemistry of garnet-bearing carbonatites of Trosø area, Norway, *Experimental geochemistry*. V. No . PP.

In connection with the problem of the existence of carbonate magmas in the upper mantle studied the phase relations and geochemistry of garnet-bearing ultra-high pressure carbonatites (UHPC) Tromsø area, Norway. UHPC is intimately associated with eclogite, carbonate-bearing phlogopite-rich garnet pyroxenite, clinopyroxene glimmerite and banded calc silicate marble. They occur in the lower parts of the Tromsø Nappe of the Caledonide orogen of Scandinavia and Greenland [Gee, Fossen et al. 2008].

Samples of UHPC have been selected during of fieldwork and research trips. The samples were studied and analyzed on a scanning electron microscope TESCAN VEGA II XMU. Trace elements in silicate and carbonate components of UHPC were determined by ICP MS in Chernogolovka. Taking into account that UHPC contain up to 20% of garnet, carbonate (Cb) and silicate (Si) components are pre-separated by chemical methods and were analyzed by ICP MS separately. Cb converted into solution by treating the powder of UHPC by 1 N solution of HCl. The insoluble residue formed on the filter after filtration of Grt was dissolved in a mixture of acids HCl, H₂SO₄, HF. The resulting solutions were analyzed. Results of the analysis characterized the concentration of trace elements in the Cb and Grt of UHPC. Concentration of SiO₂ in Cb (<n10⁻² wt.%) indicate low solubility of Grt in HCl solution during the procedure of separating Cb from UHPC. The calculation of the Si balance between UHPC and Cb (assuming that the source of Si in Cb was Grt), shows that the proportion of dissolved Grt not exceeds hundredths of %.

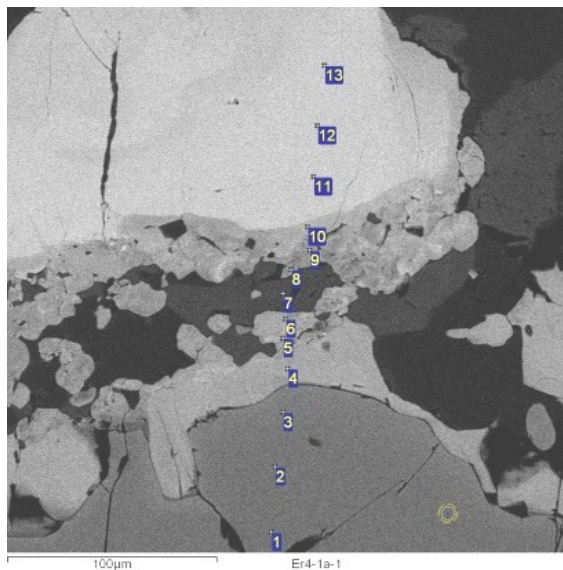
The matrix of UHPC is represented by carbonate calcite-dolomite composition with inclusions of garnet (Grt) and accessory minerals - apatite, sphene, ilmenite, rutile. On structure and composition it is allocated three generation of Grt: early, Grt₁, of pyr₁₅-gros₂₅-alm₆₀ composition, depleted in REE (< 2·10⁻² wt.%); reacting Grt_{2,3} of pyr₅-gros₆₅-alm₃₀ composition, anomalously enriched (up to 4-8 wt.%) in LREE (tabl.1, fig. 1).

The abundances of trace elements in the UHPC, it's carbonate Cb and silicate Si fraction were examination. Carbonate fraction is enriched in Ba, Rb, Nb, Sr, P, Zr, depleted in Hf, Ti, Th, Ta compared to silicate fraction (tabl. 2, fig. 2, 3).

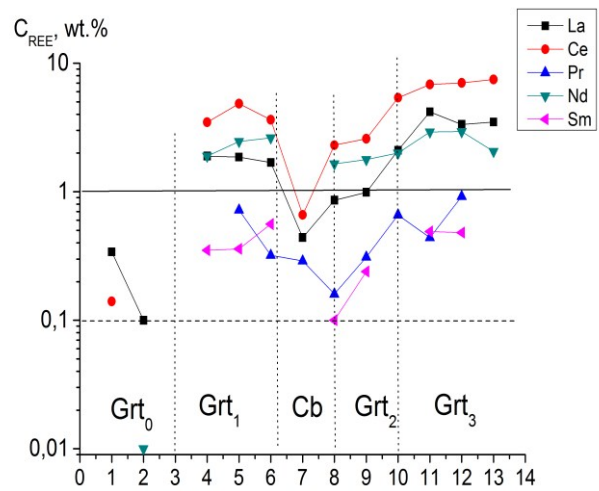
Abstracts

Table 1. Chemical composition (wt.%) of Grt, Cb and UHPC rock

	Dol	Cal	Grt ₀	Grt ₁	Grt ₂	Grt ₃	UHPC
SiO ₂	0.13	-	39.83	35.58	35.99	34.74	15.48
TiO ₂	0.21	0.09	-	0.14	0.17	-	0.69
Al ₂ O ₃	0.16	0.06	21.92	22.48	22.47	22.03	5.16
FeO	6.82	2.10	25.29	9.75	9.13	8.93	1.44
MnO	0.13	0.34	0.31	-	-	0.02	-
MgO	16.50	1.79	5.04	0.77	0.96	1.69	5.65
CaO	28.97	49.14	10.49	19.17	17.63	15.95	35.36
Na ₂ O	0.21	-	0.22	-	0.13	0.04	2.18
K ₂ O	-	-	-	-	-	0.18	1.51
Cr ₂ O ₃	0.10	-	-	-	0.07	0.07	-
SrO	0.31	0.74	0.40	1.40	1.27	1.05	-
Y ₂ O ₃	0.27	0.37	0.09	0.43	0.51	0.29	-
La ₂ O ₃	0.45	0.45	-	1.67	1.82	4.06	-
Ce ₂ O ₃	0.01	0.07	-	4.63	4.98	7.41	-
Pr ₂ O ₃	-	0.02	-	0.33	0.77	0.54	-
Nd ₂ O ₃	0.05	-	-	2.11	2.57	2.81	-
Sm ₂ O ₃	0.04	-	-	0.35	0.11	-	-
Total	54.36	55.18	103.60	98.82	98.52	99.81	67.47



a)



b)

Fig.1. UHPC: a) Back-scattered electron (BSE) images showing the zonal Grt in carbonatic matrix calcite-dolomite composition; b) distribution of LREE for profile 1-13.

Table 2. Content of trace and REE in UHPC, in Cb и Si components (ICP MS, ppm)

	UHPC	Cb component	Si component
Li	5.1	8.7	2.8
K	13689	25337	3206
Rb	43.4	109	8.7
Cs	0.00	2.8	0.22
Pb	16.4	36.2	4.9
Ba	1363	2765	241
Th	2.6	1.1	4.0
U	0.78	0.50	1.0
Nb	10.1	3.6	16.3
La	146	16.9	252
Ce	339	53.3	539

Mineral equilibria at high PT-parameters

	UHPC	Cb component	Si component
Sr	1832	3772	190
Pr	43.5	9.3	69.0
Nd	174	57.9	239
Zr	18.0	1.8	18.6
Sm	29.8	18.1	36.3
Eu	6.5	4.3	6.8
Gd	23.3	20.4	24.7
Tb	3.0	2.7	3.4
Ti	14080	9574	18527
Dy	14.6	12.0	16.1
Y	63.9	51.4	64.8
Ho	2.3	1.8	2.7
Er	5.0	3.5	6.0
Tm	0.53	0.33	0.66
Yb	2.8	1.8	3.7
Lu	0.34	0.22	0.44
Sc	42.2	11.6	60.9
V	246	235	296
Zn	159.7	200	137

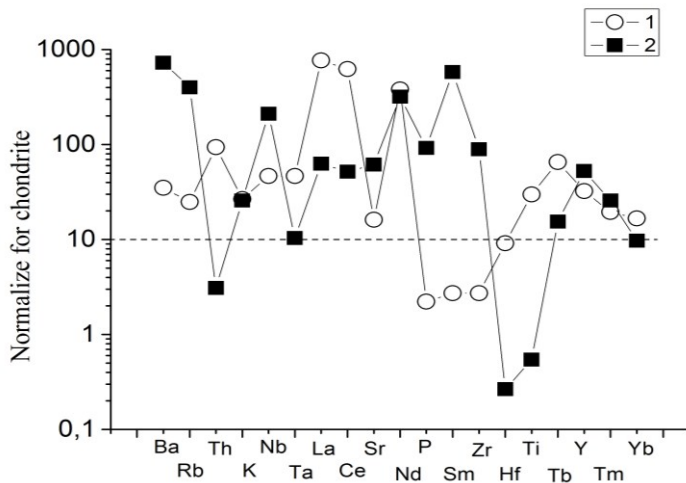


Fig. 2. Normalize for chondrite [McDonough, Sun, 1995] concentration of trace elements in carbonate Cb and silicate Si components of UHPC.

Carbonate and silicate fraction of UHPC differ in REE concentrations and the character of its dependence from atomic number N REE. Silicate fraction enriched in REE, the dependence of the normalized for chondrite REE concentrations CN from N REE has negative slope with slight Eu minimum. In the carbonate fraction to the dependence of CN-N REE has an extreme character with maximum at Gd-Tb. The largest differences are observed in the distribution of LREE. In the silicate fraction CN REE reduced from 500 at La to 50 for Sm, in carbonate fraction CN REE rise from 30 to 45 at La to Sm. Starting from Gd to Lu REE behavior is similar in silicate fraction CN REE reduced to 8, and in carbonate C fraction up to 5 (fig. 3).

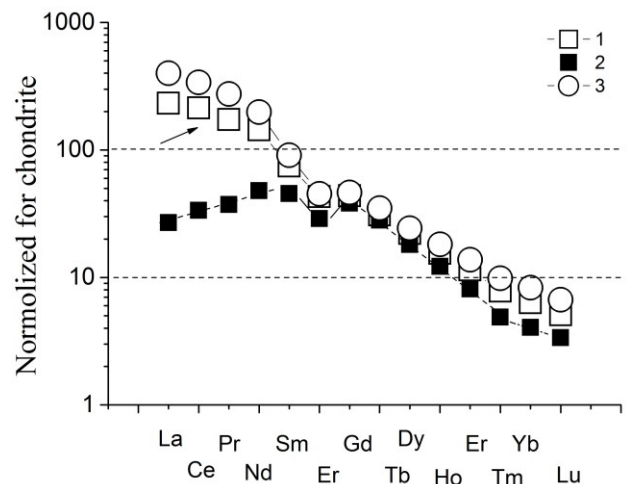


Fig. 3. Normalize for chondrite [McDonough, Sun, 1995] concentration of REE in UHPC (1), its carbonate (2) and silicate (3) components.

On the fig. 4 and 5 show ratio of trace and REE between Si and Cb components of UHPC. These data more effective show difference in distribution of these elements.

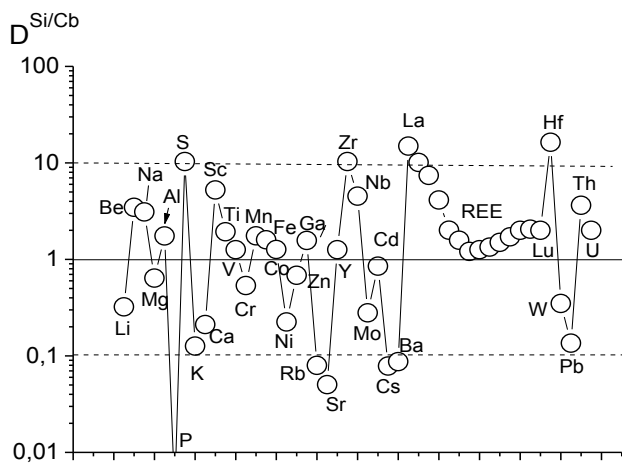


Fig. 4. Distribution (D Si/Cb) of trace elements between silicate and carbonate components of UHPC.

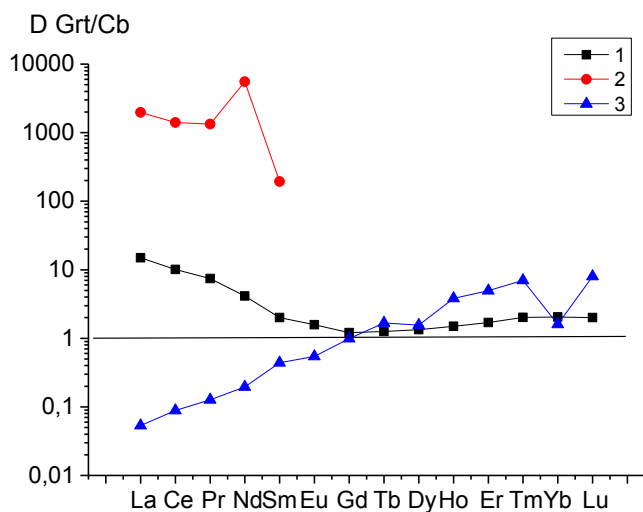


Fig. 5. Distributon of REE between silicate and carbonate components fraction of UHPC (1) , D REE Si/Cb; secondary, enrich in LREE Grt_{1,3} (2) and partition coefficients REE between Grt and carbonatite melt (D REE Grt/CbL) our experimental data, T= 1250°C, P=4 GPa [Gorbachev et al., 2014]

The anomalous distribution of REE is observed between Si and Cb components in UHPC compared with experimental D REE Grt /CbL. Since, in the Si component of UHPC dominated Grt, it can be assumed that the ratio of rare earth elements between Si and Cb components of UHPC R Si/Cb characterizes the combined distribution coefficients D REE between Grt and CbL: R Si/Cb ~ D Grt/CbL. However, as can be seen from Fig. 5, R Si/Cb in UHPC differ from the experimental D Grt/CbL. Dependence R Si/Cb in UHPC has an extreme

character with a minimum in the field of Gd, decreasing from La to Gd, and gradually increasing to Lu. According to experimental data D REE Grt/CbL increases from La to Lu. Relationship between R REE Grt₂ , enriched in LREE and Cb even more different from the experimental D REE Grt/CbL (Fig. 5). This feature can be explained as enrichment of the later generations of garnet Grt₂ and Grt₃ by LREE under the influence of carbonatite melt into the primary mantle material under non-equilibrium conditions.

This work was supported by RFBR grant №14-05-00752a.

References:

1. Gee D.G, Fossen H., Henriksen N., Higgins A.K. (2008) From the early Paleozoic platforms of Baltica and Laurentia to the Caledonide orogen of Scandinavia and Greenland. *Epizodes*. V.31, N.1. P. 44-51
2. Gorbachev N.S, A.V Kostyuk (2014) Distribution of rare and rare earth elements between Grt, Cpx and Cb at mantle PT (from experimental data). *Experimental geochemistry*. T.2. №2. C. 70-72
3. McDonough W.F., Sun S. (1995) The composition of the Earth. *Chemical Geology*. 120. 223-253.

Gorbachev¹N.S., Kostyuk¹A.V., Ravna²E., Nekrasov¹A.N., Kullerud²K. The melting of ultra-high-pressure garnetbearing carbonatite (UHPC) of Tromsø area, Norway, at mantle PT

¹Institute of Experimental Mineralogy RAS, Chernogolovka Moscow district

²University Tromsø, Norway

Abstract. Melting of ultra-high-pressure garnet-bearing carbonatite (UHPC) in "dry" conditions and with H₂O+CO₂ fluid experimentally studied at P = 4 GPa in the range T = 950-1400°C. The temperature of the "dry" liquidus UHPC is about 1270°C, T of solidus ~ 1050°C. Liquidus and solidus temperatures drop to 100-150°C during melting with H₂O+CO₂ fluid. At T = 1400°C observed separation of carbonatite melt on high- and low-calcium carbonate-silicate liquid with separation of graphite. In sub-liquidus fields carbonatite melt reacts with Grt, thereby forming a bordure of reaction Grt, enriched in CaO, TiO₂, SrO, depleted in FeO, MgO, MnO. The experimental results indicate the formation of characteristic UHPC association of carbonate- zone garnet in the range of T = 1200-1250°C.

Keywords: *experiment, melting, phase relationship, high PT carbonatite*

Citation: Gorbachev N.S., A.V. Kostyuk, E. Ravna, A.N. Nekrasov., K. Kullerud (2015) The melting of ultra-high-pressure garnet-bearing carbonatite (UHPC) of Tromsø area, Norway, at mantle PT. *Experimental geochemistry*. V. No . PP.

Particular phase relationships at melting of UHPC in "dry" conditions and with H₂O+CO₂ fluid experimentally studied at P = 4 GPa in the range T = 950-1400°C to determine the physical and chemical conditions of formation UHPC.

Mineral equilibria at high PT-parameters

Table 1. The composition of coexisting phases of UHPC from experiments on peridotite melting

P = 4.0 GPa, T = 950°C, "dry" system												
	SiO ₂	TiO ₂	Al ₂ O ₃	FeO	MnO	MgO	CaO	Na ₂ O	K ₂ O	P ₂ O ₅	Cr ₂ O ₃	Total
Cal	0.02	0.11	0.07	3.31	0.10	2.90	47.17	0.04	0.02	0.06	0.00	54.26
Cpx	52.32	0.31	3.38	10.82	0.20	10.73	20.48	1.90	0.18	0.00	0.03	100.50
K-Cpx	45.88	1.35	6.53	11.69	0.11	10.87	12.78	1.48	2.71	0.18	0.01	94.07
Bt	39.87	3.55	13.73	15.48	0.04	14.23	0.50	0.22	9.94	0.00	0.00	97.58
Grt	38.24	0.71	19.99	22.33	0.71	4.96	12.54	0.17	0.08	0.08	0.12	100.36
P = 4.0 GPa, T = 950°C, H ₂ O+CO ₂ fluid												
Cal	0.16	0.11	0.07	4.13	0.08	3.40	45.94	0.03	0.12	0.25	0.07	55.25
CbL	2.23	0.02	0.09	5.04	0.00	4.10	43.39	0.05	0.16	0.49	0.01	55.57
Cpx	53.64	0.06	1.48	7.76	0.10	14.35	23.10	0.12	0.06	0.12	0.07	101.62
Grt	38.50	0.10	20.66	25.28	0.71	4.17	11.16	0.12	0.00	0.00	0.00	100.94
Bt	40.46	3.38	13.97	12.39	0.00	16.77	0.54	0.00	10.22	0.00	0.00	97.88
P = 4.0 GPa, T = 1050°C, "dry" system												
Cb	0.06	0.06	0.00	2.42	0.25	1.50	49.56	0.10	0.16	0.19	0.00	55.22
Grt	37.96	1.07	20.13	16.51	0.39	5.46	17.22	0.00	0.00	0.08	0.35	99.36
Cpx	50.53	0.49	3.37	8.76	0.23	12.14	22.54	0.45	0.04	0.04	0.08	98.66
P = 4.0 GPa, T = 1050°C, H ₂ O+CO ₂ fluid												
CbL	0.38	0.08	0.00	1.49	0.15	1.34	50.47	0.02	0.21	0.68	0.00	55.63
Grt	38.64	1.09	21.14	13.35	0.45	6.88	18.46	0.00	0.11	0.30	0.06	100.53
Bt	40.34	2.88	13.98	14.28	0.00	15.30	1.24	0.24	9.22	0.08	0.00	97.95
P = 4.0 GPa, T = 1150°C, "dry" system												
CbL	0.36	0.20	0.15	2.90	0.31	1.17	47.27	0.00	0.27	0.60	0.00	53.50
Grt	38.03	0.92	20.44	14.34	0.38	6.84	15.89	0.00	0.08	0.00	0.09	97.11
Cpx	49.11	0.43	5.57	7.03	0.15	12.30	21.80	0.74	0.00	0.00	0.00	97.36
Bt	34.65	6.26	11.55	18.12	0.08	10.16	2.55	0.14	9.08	0.98	0.05	93.89
P = 4.0 GPa, T = 1150°C, H ₂ O+CO ₂ fluid												
CbSiL	11.88	1.27	4.17	6.40	0.26	4.97	32.27	0.27	1.92	2.20	0.00	66.67
Grt	37.47	1.38	20.17	17.60	0.66	6.14	14.25	0.10	0.05	0.11	0.10	98.65
Bt	30.59	3.22	11.29	13.15	0.08	9.96	9.35	0.39	6.25	3.30	0.01	88.78
P = 4.0 GPa, T = 1250°C, H ₂ O+CO ₂ fluid												
Gr _{t,c}	37.76	0.02	20.21	26.45	0.78	4.23	10.54	0.02	0.00	0.00	0.21	100.26
Gr _{t,r}	40.20	0.36	22.26	13.21	0.68	10.45	13.15	0.08	0.00	0.00	0.22	100.61
CbSiL	14.47	1.00	2.92	8.63	0.09	7.22	30.01	0.77	0.57	5.66	0.00	71.40
Si	33.35	1.81	10.81	9.57	0.27	6.12	17.27	1.01	1.67	1.61	0.08	83.58
Cb	9.98	0.06	1.25	7.29	0.15	7.72	34.10	0.29	0.33	4.76	0.00	66.01
P = 4.0 GPa, T = 1300°C, "dry" system												
CbL	23.13	2.23	4.72	4.79	0.10	4.81	35.10	0.92	0.14	10.71	0.03	85.98
Gr _{t,1}	37.73	0.28	20.58	25.11	1.10	4.14	11.14	0.03	0.03	0.07	0.00	100.20
Gr _{t,2}	39.10	0.93	22.05	11.68	0.37	8.62	16.49	0.15	0.07	0.19	0.17	99.82
P = 4.0 GPa, T = 1300°C, H ₂ O+CO ₂ fluid												
CbSiL	15.43	0.78	5.32	1.94	0.15	5.34	33.95	0.60	1.40	2.26	0.14	67.51
Si	28.96	1.65	10.21	3.67	0.05	13.06	15.42	0.69	5.03	5.34	0.14	84.40
Cb	4.01	0.32	1.57	0.86	0.09	3.51	42.82	0.15	0.68	0.31	0.00	54.35
P = 4.0 GPa, T = 1400°C, H ₂ O+CO ₂ fluid												
L ₁ (matr)	24.29	2.33	8.82	7.06	0.30	6.97	25.60	0.39	2.48	3.44	0.08	82.22
L ₂	20.01	1.96	7.36	5.83	0.03	5.49	25.37	0.38	1.83	2.03	0.09	71.91

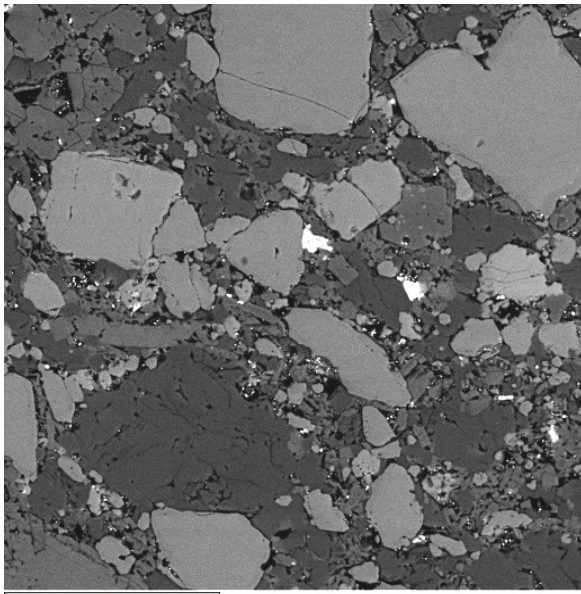
Note: (here and below) Cal - calcite, CbL - carbonate melt, Cpx - clinopyroxene, K-Cpx - potassium-bearing clinopyroxene, Bt - biotite, Grt - garnet, CbSiL - carbonatite melt, Si - silicate component, Cb - carbonate component, L - melt.

Abstracts

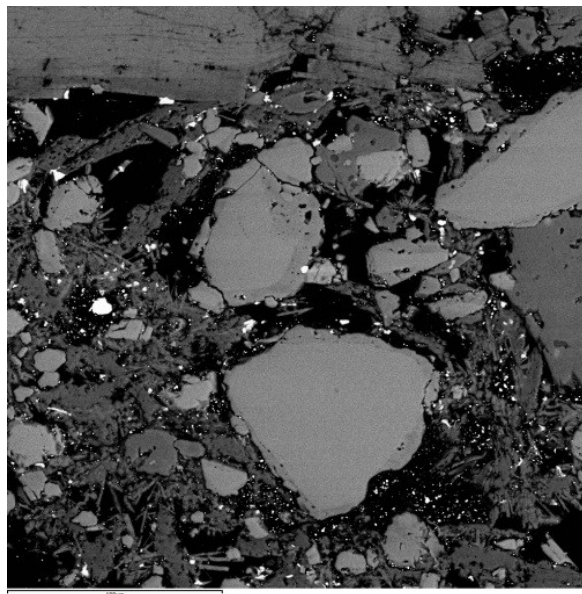
Experiments were carried out on the anvil-with-hole apparatus by quenching technique with Au, Au-Pd and Pt ampoules [Gorbachev, 1990] in the IEM RAS. Fine powders of Grt-containing carbonatite of UHPC was the starting material; a source of H_2O+CO_2 (15 wt.%) - oxalic acid dihydrate $H_2C_2O_4 \cdot 2H_2O$. Phase composition and geochemistry of UHPC are given in this issue [Gorbachev and others, 2015]. The temperature was measured by Pt30Rh/Pt6Rh thermocouple, pressure at high temperatures calibrated for the equilibrium curve of quartz - coesite [Litvin, 1991]. Products of

experiments were studied using electron probe microanalysis on a digital scanning electron microscope Tescan VEGA TS 5130MM. The results are shown in Table 1 and Fig. 1-4.

The temperature of "dry" solidus is about $1050^\circ C$. Composition of sub-solidus association at $T = 950^\circ C$ is Cb, Cpx, KCpx, Grt, and accessory minerals (AM) - Bt, Apt, Ilm, Sph. At melting with H_2O+CO_2 fluid solidus is lowered up to $T < 950^\circ C$. At $T = 950^\circ C$ carbonatite melt (CbL) coexists with Cal, Cpx, Grt, AM - Apt, Bt (Fig. 1).

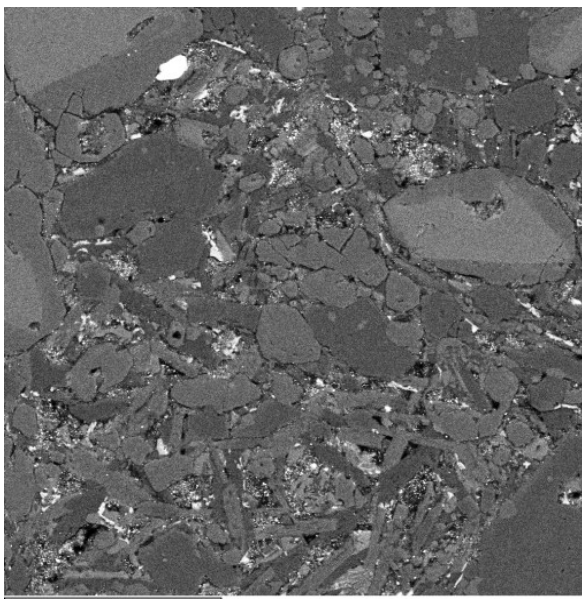


a)

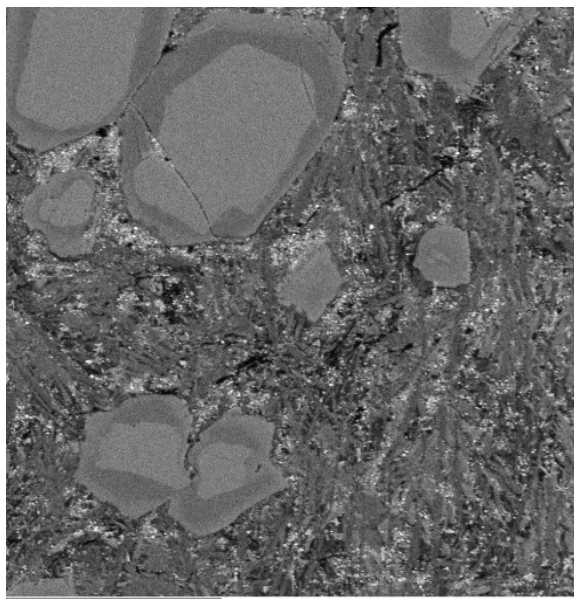


b)

Fig. 1. Microphotograph of quenching samples in BSE at $T = 950^\circ C$: a) "dry" conditions; b) H_2O+CO_2 fluid.



a)



b)

Fig.2. BSE images of quench samples at $T=1150^\circ C$: a) «dry» condition; b) H_2O+CO_2 fluid.

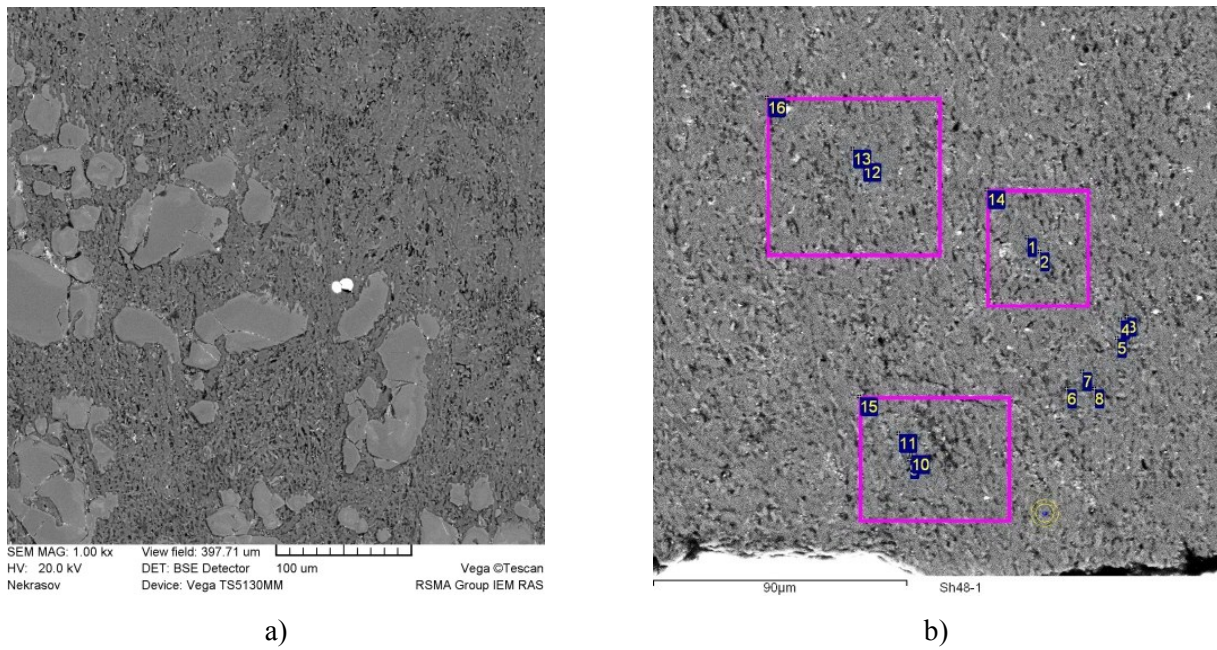


Fig. 3. BSE images of quench samples at T=1300°C: a) «dry» condition; b) H₂O+CO₂ fluid

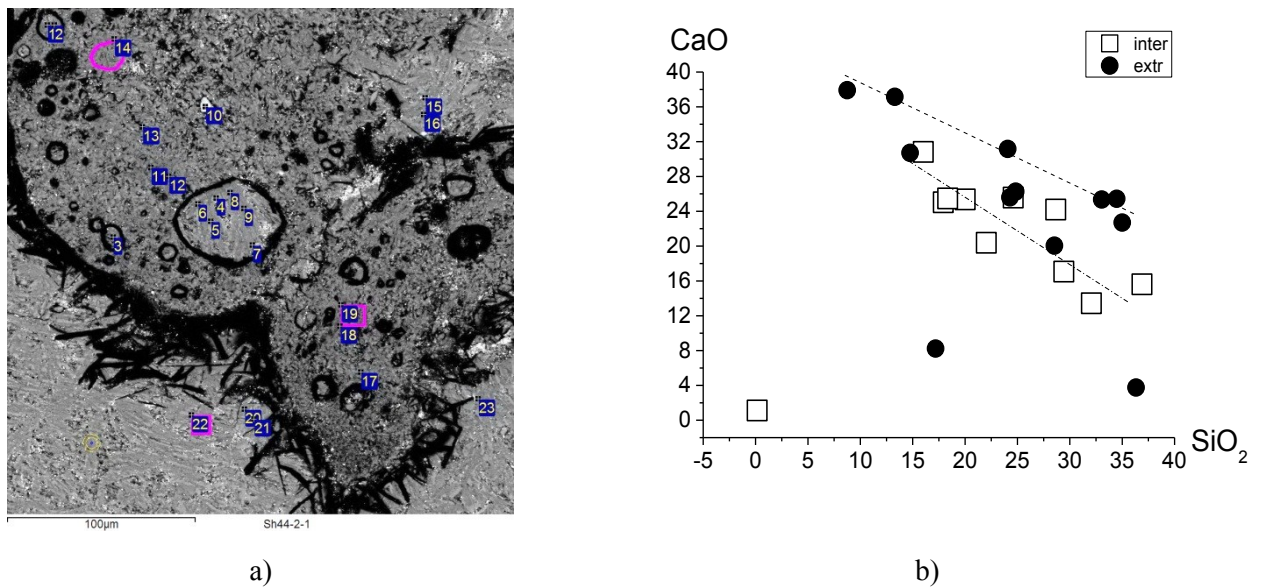


Fig.4. BSE images (a) of quench samples at T=1400°C. Stratification of carbonatite melt on high- and low-calcium carbonate-silicate liquids with separation of graphite; b) CaO-SiO₂ composition of 1 and 2 types of liquids.

At "dry" conditions in the range of temperature from 1050 to 1150°C under-solidus association presented by Cal, Grt, Spx, Bt and accessory minerals - Apt, Ilm, Rt. Cpx stable up to T ≥ 1150°C, Grt – at T ≥ 1300°C. At melting with H₂O+CO₂ fluid Cpx stable up to T = 1150°C, Grt – at T < 1250°C (Fig. 2).

At T = 1300°C in "dry" conditions carbonatite melt (CbL) coexists with zone Grt. Full melting was observed at T > 1150 and < 1250°C in the system with H₂O+CO₂ fluid. Mixture of microlites a of variable composition from carbonate-silicate (CbSi) to silicate-carbonate (SiCb) formed at quenching of under-liquidus carbonate-silicate melt (CbSiL) (Fig. 3).

Stratification of carbonatized silicate melt on high- and low-calcium carbonate-silicate liquid with separation of graphite observed at T = 1400°C (Fig. 4).

Thus, melting of UHPC occurs in a wide range of T in "dry" conditions from 1050°C up to 1300°C. The temperature of the "dry" liquidus UHPC is about 1270°C, T of solidus ~ 1050°C. At melting of UHPC with H₂O+CO₂ fluid T of liquidus is lowered to 1200°C, solidus - to 950°C. In sub-liquidus fields carbonatite melt reacts with Grt, thereby forming a bordure of reaction Grt, enriched in CaO, TiO₂, SrO, depleted in FeO, MgO, MnO. Stratification of carbonatite melt on high- and low-calcium carbonate-silicate liquid with separation of graphite observed at T = 1400°C, P = 4 GPa in the system with H₂O+CO₂

fluid. The experimental results indicate the formation of characteristic UHPC association of carbonate-zone garnet in the range of $T = 1200-1250^{\circ}\text{C}$.

This work was supported by RFBR grant №14-05-00752a.

References:

1. Gorbachev N.S. (1990). Fluid-magma interaction in sulfide-silicate systems. Intern Geology Review. V.32, N.8, P. 749-831
2. Gorbachev N.S., E. Ravna, A.V. Kostyuk, A.N. Nekrasov., K. Kullerud (2015) Phase relationship and geochemistry of garnet-bearing carbonatites of Trosø area, Norway, Experiment in geochemistry.
3. Litvin Yu.A. (1991). Physico-chemical studies of the deep melting of the Earth. M. Science.

Gorbachev N.S., Kostyuk A.V., Nekrasov A.N. Interaction of basaltic melt with peridotite: effect of fluid on phase relations (for experimental datas)

Institute of Experimental Mineralogy RAS, Chernogolovka Moscow district

Abstract. Interaction basalt melt-peridotite in the range $P = 1.0-2.5$ GPa, $T=1250-1300^{\circ}\text{C}$ with H_2O and $\text{H}_2\text{O}+\text{CO}_2$ fluid and with use Pt-peridotite ampoules is experimentally studied. At interaction pyroxenization of peridotite with replacement of Ol to Opx was observed. The volume of melts is defined by volume basalt components. In the presence of fluid magnesian melts are formed at lower temperatures - on 200°C and more, than in "dry" conditions. Ol-Opx replacement it is possible to explain by high activity SiO_2 and Al_2O_3 in basalt melt at which Ol becomes unstable.

Key words: *experiment, high pressure, basalt melt, peridotite, interaction, fluid.*

Citation: Gorbachev N.S., A.V Kostyuk., A.N.Nekrasov Interaction of basaltic melt with peridotite: effect of fluid on phase relations (for experimental datas). *Experimental Geochemistry*. T. №. P.X-XX

http://exp-geochem.ru/JPdf/201X/XX/XXXXXX_rus.pdf

Interaction basalt melts with peridotite plays the important role in processes magma formation at partial melting substance of upper mantle, mantle plumes, subduction of oceanic slab and overlying mantle wedge. Existing experimental data are executed basically by method of joint solubility «the dissolution couple method» or sandwich method in "dry", without fluid addition, conditions. It has been shown, that the composition of melts influences on solubility peridotite in melts and structure of reactionary zone between melt and peridotite [Wang et.al, 2013; Yaxley, 2000; Mallik et.al, 2012]. High T (from 1450 to 1700°C) at which were made experiments are caused high T solidus "dry"

peridotite-basalt mixture. Fluid effective influence on T melting of peridotite-basalt mixture and phase composition at interaction basalt melt with peridotite. The main results of such influence consist in essential (on 200°C and more) decrease T of formation magnesian melts in comparison with melting of "dry" peridotite or peridotite-basalt mixture and pyroxenization of peridotite [Gorbachev, 2010].

Effect of H_2O and $\text{H}_2\text{O}+\text{CO}_2$ fluid on phase relationship at interaction basalt melt-peridotite with H_2O and $\text{H}_2\text{O}+\text{CO}_2$ fluid in the range $P = 1.0-2.5$ GPa, $T = 1250-1300^{\circ}\text{C}$ were experimental studying.

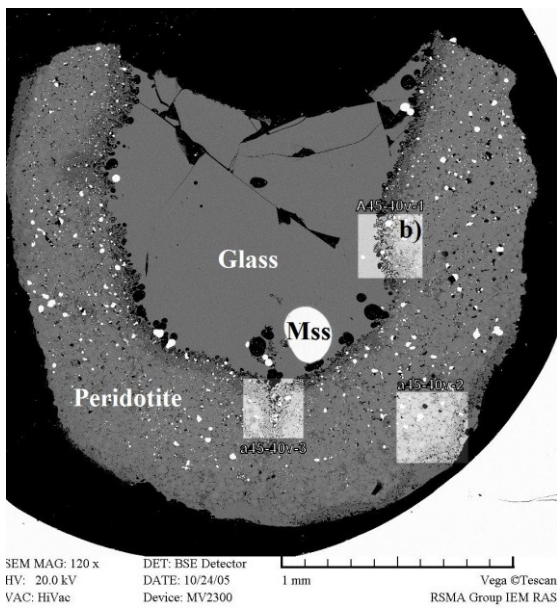
Experiments were carried out in IEM Russian Academy of Sciences on of the piston-cylinder equipment with use Pt-peridotite ampoules [Gorbachev, 1990]. The investigated samples consisted from specially prepared by moulding and sintering in inert atmosphere peridotite ampoules. The ampoule was densely filled with a thin powder of the initial sample consisting of a mechanical mix of basalt, synthetic sulphide Fe-Ni-Cu (Mss). Peridotite ampoule were located into platinum ampoule which was hermetically sialed. After quench ampoule sawed in longitudinal direction, each of which in a special compression mould under pressure and heating press in polystyrene. From the received tablet prepared the polished preparations which were studied and analyzed using electron probe microanalysis on a digital scanning electron microscope Tescan VEGA TS 5130MM. For peridotite ampoules served as an initial material spinel peridotite from xenolite of kimberlite pape [Ukhanov, etc., 1988], toleitic basalt of average trapp composition. H_2O -флюид it was set by distilled water. As source $\text{H}_2\text{O}+\text{CO}_2$ fluid served $\text{H}_2\text{C}_2\text{O}_4 \times 2\text{H}_2\text{O}$. Concentration of a fluid component - $5-7$ wt. %. Internal association Ol-Opx-Sp-Pt-PtS-silicate and sulfide melts supervised of f_{S_2} and f_{O_2} . Temperature measured Pt30Rh/Pt6/Rh by the thermocouple, pressure calibrated on a curve of equilibrium quartz-koesit. Accuracy of definition of temperature and pressure is estimated in $\pm 10^{\circ}\text{C}$ and ± 1 kbar [Litvin, 1991]. Duration of experiment made 6-8 hours.

Results of experiments are resulted on fig. 1-3 and in table 1. Experimental samples consisted from peridotite ampoule filled with silicate glass, product of melting initial basalt, with distinct reactionary border between internal part peridotite ampoules and silicate glass in ampoule The share reacted with basalt melt peridotite did not exceed 1/10 parts of a thickness of an ampoule (fig. 1).

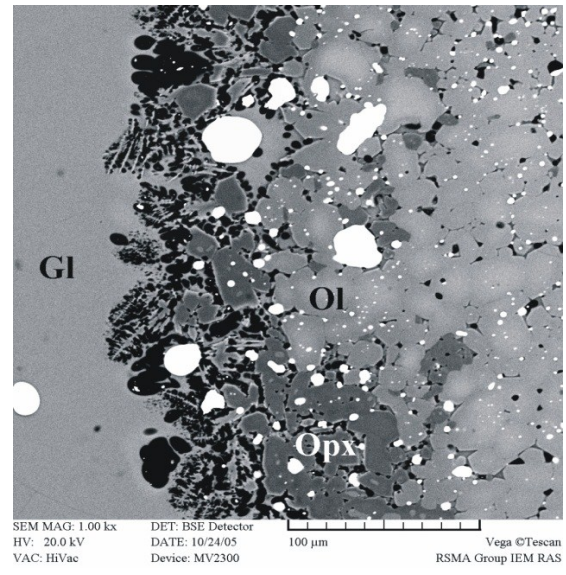
Mineral equilibria at high PT-parameters

Table 1. Compositions of coexist phases of experimental samples

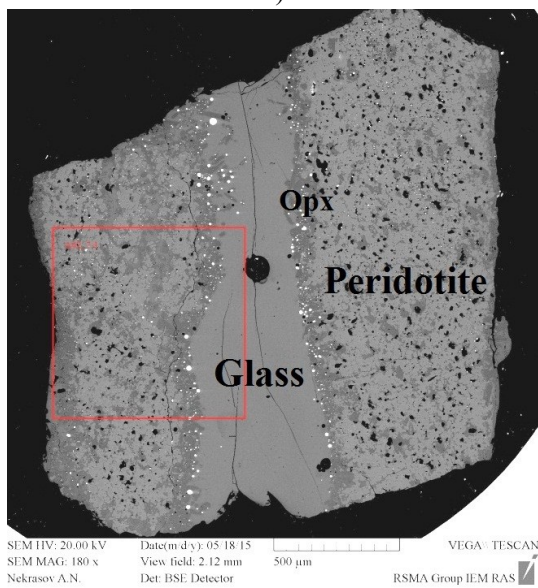
	SiO ₂	TiO ₂	Al ₂ O ₃	FeO	MnO	MgO	CaO	Na ₂ O	SO ₃	Total
P = 1.0 GPa, T = 1300°C, H₂O-fluid										
L_{Sil}	45.52	1.19	9.84	14.35	0.20	11.74	6.83	1.64	0.72	92.03
Opx	54.31	0.19	1.64	9.58	0.19	29.79	1.19	0.00	0.00	96.89
Ol	37.47	0.08	0.00	15.58	0.15	45.15	0.10	0.13	0.14	98.80
P = 1.3 GPa, T = 1250°C, H₂O+CO₂- fluid										
L_{Sil}	46.45	1.85	12.60	9.25	0.26	8.48	10.13	2.29	0.12	91.45
Opx	50.40	0.97	8.58	10.49	0.22	21.98	5.00	0.42	0.05	98.31
Ol	37.22	0.00	0.22	14.55	0.00	47.31	0.01	0.14	0.00	99.45
T = 1250°C, P = 2.5 GPa, H₂O+CO₂- fluid										
L_{Sil}	45.90	2.09	12.91	14.43	0.17	6.23	8.26	2.26	0.36	92.61
Cpx	49.13	0.76	10.09	10.53	0.40	14.44	12.32	1.32	0.00	98.99
Opx	49.89	0.00	3.93	11.09	0.00	29.08	1.42	0.22	0.12	95.75
Ol	38.24	0.00	0.40	16.01	0.27	45.53	0.08	0.33	0.05	100.91



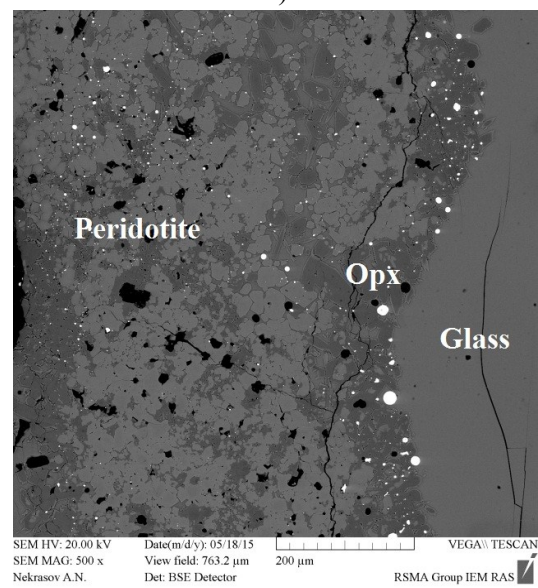
a)



b)

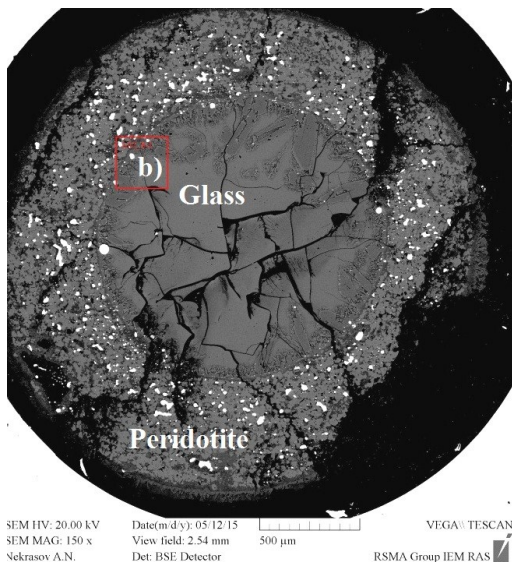


c)

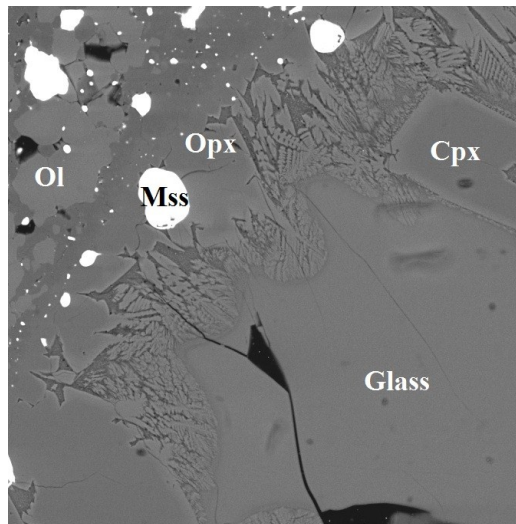


d)

Fig. 1. BSE image of run samples. (a-b) P = 1.0 GPa, T = 1300°C, H₂O-fluid; (c-d) P = 1.3 GPa, T = 1250°C, H₂O+CO₂- fluid.



a)



b)

Fig. 2. BSE image of run sample. (a) panoptic of run sample, peridotite ampoule filled with silicate glass; (b) contact of silicate glass with peridotite ampoule. T = 1250°C, P = 2.5 GPa, H₂O+CO₂-fluid.

In all experiments in a cross-section of the quenchen sample zonality was observed. The composition of zones from central part of ampoule to peridotite are: silicate glass - reactionary and quenchen zone Cpx-Opx composition (an internal "basalt" part of the sample), Opx zone-Ol of peridotite ampoule with intergrain silicate glass (peridotite part of ampoule). Content of MgO in reactionary melts decreased from 8-10 wt.% at H₂O+CO₂ fluid up to 12-14 wt. %, at H₂O fluid, Content of FeO varied from 12 to 14 wt. %.

Thus, the main results of influence fluid on interaction basalt melt with peridotite in depend on type of fluid, consist in essential (more than 200°C) decrease in temperature of formation magnesian melts in comparison with melting peridotite ore peridotite-basalt source in "dry" conditions and pyroxenisation of peridotite. As H₂O in more degrees reduces T melting of silicates, increasing thereby degrees of melting of peridotite and more magnesian melts are formed at H₂O fluid. The volume of melts is defined by volume basalt components in a source.

Ol on liquidus of fluidbearing magnesian basalts melts and its replacement pyroxenes absence it is possible to explain high activity SiO₂ and Al₂O₃ in basalt melt at which Ol becomes unstable. On fig. 3 phase equilibrium in system SiO₂-MgO-CaO-Al₂O₃ depending on activity SiO₂ and Al₂O₃ calculated proceeding from rules of construction of multisystems [Zharikov, 2005] are resulted.

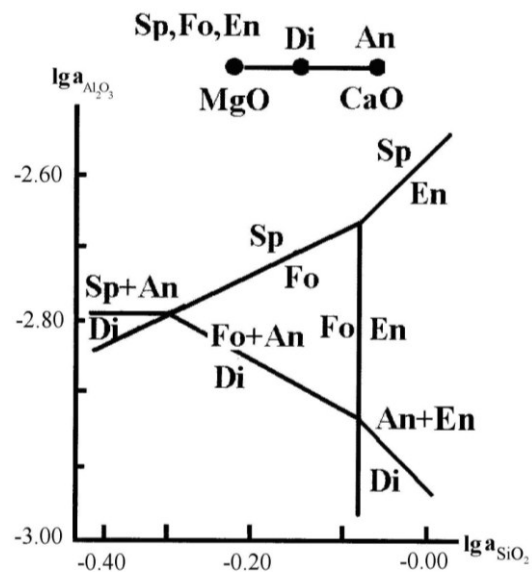


Fig. 3. Phase relations in system SiO₂-MgO-CaO-Al₂O₃ in depend on activity SiO₂ and Al₂O₃ in basalt melt, with peridotite interacted.

The diagramme calculate with use of thermodynamic data [Robi et al., 1979] proceeding from an assumption, that relations activity pure minals in minerals are equal 1. From the diagramme limitation field of stability Ol and critical values of activity SiO₂ and Al₂O₃ in melt, at which achievement, Fo it is replaced pyroxenes and spinel is visible. Signs Ol-less liquidus magnesian mantle magmas meet in various geological objects (pyritic basalts of gd suite Sibirean trapp of Norilsk area [Gorbachev, 2010], basalts of the Hawaiian volcanoes [Sobolev, 2007].

Supporting by grant RFBR №14-05-00752a.

References:

1. Gorbachev N.S. (2010) Experimental study of interaction of fluidbearing basaltic melts with peridotite: mantle-crust interaction at trapp magmatism of Norilsk area. *J. Petrology*, T. 18. №. 4. P. 416-431.
2. Zharikov V.A. (2005). Basics of physico-chemical petrology. Vanity press Moscov University.
3. Litvin Y.A. (1991). Physico-chemical investigations of melting deep matter of Earhs. M. Nauka.
4. Gorbachev N.S. (1990) Fluid-magma interaction in sulfide-silicate systems. *Intern Geology Review*. V.32, N.8, P. 749-831
5. Mallik A, Dasgupta R (2012) Reaction between MORB-eclogite derived melts and fertile peridotite and generation of ocean island basalts. *Earth Planet Sci Lett* 329–330:97–108
6. Robi R.A., B.S. Hemingway, J.R. Fisher (1979) Thermodynamic properties of minerals and related substances at 298.15 K and 1 bar (10^5 Pascals) pressure and at higher temperatures. *U.S. Geol. Survey Bullet.* 142.
7. Sobolev A.V., Hofmann A.W., Kuzmin D.V. et al. (2007) The amount of recycled crust in sources of mantle-derived melts // *Science*. V. 316. № 5823. P. 412-417.
8. Ukhanov A.V., Rjabchikov I.D., Kharkiv A.D. (1988) Lithospheric mantle of the Yakutian kimberlite province. Moscow. "Nauka".
9. Wang C., Y. Liang, W. Xu, N. Dygert (2013) Effect of melt composition on basalt and peridotite interaction: laboratory dissolution experiments with applications to mineral compositional variations in mantle xenoliths from the North China Craton. *Contrib Mineral Petrol* 166:1469–1488. DOI 10.1007/s00410-013-0938-6
10. Yaxley G.M. (2000) Experimental study of the phase and melting relations of homogeneous basalt + peridotite mixtures and implications for the petrogenesis of flood basalts. *Contrib Mineral Petrol*. 139: 326-338

Kostyuk A.V., Gorbachev N.S., Nekrasov A.N. Experimental study of peridotite - basalt - $(K, Na)_2CO_3$ -fluid system: the influence of T, P and fluid composition on the solubility of accessory minerals in silicate melts

Institute of Experimental Mineralogy RAS, Chernogolovka Moscow district

Abstract. Solubility of accessory minerals (AM) in "dry" and fluid-containing (H_2O , H_2O+CO_2) silicate melts studied experimentally in the peridotite-basalt- $(K, Na)_2CO_3$ system, at $T=1100-1250^\circ C$ and $P = 0.3-0.5$ and 4.0 GPa. Experiments were carried out in an internal-heated pressure vessels and on the anvil-with-hole apparatus in IEM RAS. Products of experiment have been studied on a microprobe. Experimental results showed that solubility of AM depends on T, P and fluid composition. At crust PT ($0.3 - 0.5$ GPa) in H_2O+CO_2 -containing silicate melts solubility of AM higher than in H_2O -containing melts. With

T increases from 1100 to $1250^\circ C$ concentration of ZrO_2 and TiO_2 increases, concentration of SO_3 and P_2O_5 decreased at saturation conditions. At P increases from 0.3 to 0.5 GPa ($T = 1250^\circ C$) the solubility of all AM decreases. Silicate-carbonate-sulphide stratification of silicate melt observed at the mantle PT (4 GPa). The distribution coefficients (K_D) between carbonate and silicate melts shows that Zr, S, P, Na, Mn, Ca >1 ; Ti, Cr, Si, Al, K, Mg, Fe < 1 .

Keywords: *experiment, geochemistry, solubility, melts, accessory minerals, fluid.*

Citation: Kostyuk A.V., N.S.Gorbachev, A.N.Nekrasov. 2015. Experimental study of peridotite-basalt- $(K, Na)_2CO_3$ -fluid system: the influence of T, P and fluid composition on the solubility of accessory minerals in silicate melts. *Experimental geochemistry*.. V. 3. No . PP.

The accessory minerals (AM) are important concentrators of trace elements in magmatic rocks of different origins. They define their behavior in the formation and differentiation of the magmas. The main concentrators of P, S, Ti, Zr, Cr are apatite, pyrrhotite, ilmenite, zircon and chromite respectively. The concentrations of each of these elements in the melt are determined solubility of minerals concentrators. At experimental study of the influence of physical and chemical conditions on the phase relationship at partial melting of peridotite-basalt- $(K, Na)_2CO_3$ -fluid system were obtained data which characterizing the solubility AM in "dry" and fluid-containing (H_2O , H_2O+CO_2) silicate melts at $T = 1100-1250^\circ C$, $P = 4.0$ and $0.3-0.5$ GPa.

(1) Experiments at $P = 0.3-0.5$ GPa, $T=1100-1250^\circ C$ were carried out in an internal-heated pressure vessels in the IEM RAS. On the gas apparatus pressure measured by a manometer with an accuracy of ± 50 atm, the temperature - by Pt30Rh/Pt6Rh thermocouple. The duration of experiments was 48 hours. Sulphur and oxygen fugacity buffered by PtPtS and CoCoO respectively. (2) Experiments at $P = 4.0$ GPa, $T = 1250^\circ C$ were carried out on the anvil-with-hole apparatus in the IEM RAS. The temperature was measured by Pt30Rh/Pt6Rh thermocouple, pressure at high temperatures calibrated for the equilibrium curve of quartz - coesite [Litvin, 1991]. Duration of experiment was 10 hours. Internal association of Ol-Opx-Sp-Pt-PtS-silicate-sulphide melt $([Fe_2SiO_4]^{Ol} + \frac{1}{2} S_2(g) = [FeSiO_3]^{Opx} + FeS (Ms) + \frac{1}{2} O_2 (g))$ controlled sulphur and oxygen fugacity.

For the experimental study of fluid- and sulphide-containing systems we used a special multi-ampoule quenching technique with peridotite ampoule [Gorbachev, 1990]. Specially prepared peridotite container protected the platinum ampoule from aggressive sulphide melt and prevented iron loss by melt during its interaction with the Pt ampoule. The peridotite of xenoliths from the kimberlite pipe Grib (Arkhangelsk region) was the starting material for the peridotite container. Container was filled by fine

Abstracts

powder of initial sample consisting of a mixture of the basalt glass (60%) - K_2CO_3 (5%) - Na_2CO_3 (5%) – with AM: Ni-containing pyrrhotite (10%) - ilmenite (5%) - apatite (5%) - chromite (5%) - a few grains of zircon (1-2 mm). Alkali carbonates (K, Na) $_2CO_3$ used because the alkaline carbonate fluid plays an important role in the mantle metasomatism, and also because of the close spatial and genetic relationship between carbonatite rocks and alkaline complexes. Peridotite container was placed in a platinum ampoule added to the system 10 wt.% of distilled H_2O or 15 wt.% of $H_2C_2O_4 \cdot 2H_2O$ (source of H_2O+CO_2) and hermetically sealed. Finished sample was placed in a buffered Pt ampoule of larger diameter.

After experiment the sample was opened and polished for microprobe study. Products of experiments were studied using electron probe microanalysis on a digital scanning electron microscope Tescan VEGA TS 5130MM.

The Fig.1 shows that original structure of the sample has remained after the experiment with visible boundaries between peridotite container ("peridotite" in Fig. 1) and glass ("basalt" in Fig.1). Results in this paper describing the phase composition of the quenching samples and focused on concentration of P, S, Ti, Zr, Cr in silicate melts coexisting with AM. Representative chemical compositions of the coexisting phases are shown in Table 1.

Table 1. Representative chemical compositions of the coexisting phases

	SiO ₂	TiO ₂	Al ₂ O ₃	FeO	MnO	MgO	CaO	Na ₂ O	K ₂ O	SO ₃	P ₂ O ₅	Cr ₂ O ₃	ZrO ₂	Total
P = 0.3 GPa, T = 1250°C, H₂O fluid														
L _{Sil}	53.43	0.83	15.25	2.54	0.13	0.58	9.72	2.51	1.19	1.73	0.82	0.13	1.28	90.11
Ol	40.87	0.08	0.40	10.65	0.17	47.10	0.35	0.10	0.08	0.06	0.34	0.17	0.08	100.43
Cpx	41.57	2.36	8.95	12.02	0.23	8.77	21.04	0.48	0.05	0.41	0.86	0.12	1.17	98.03
Phlog	44.81	2.53	12.76	11.54	0.05	11.77	3.84	1.36	5.75	1.24	0.41	0.17	0.43	96.64
Amf	44.54	1.92	12.92	10.84	0.26	5.43	13.95	1.50	1.49	1.39	0.81	0.26	1.17	96.45
P = 0.5 GPa, T = 1100°C, H₂O fluid														
L _{Sil}	50.74	0.42	16.65	1.16	0.12	0.14	8.31	2.74	1.09	1.00	0.63	0.06	0.66	83.79
Ol	40.15	0.06	0.31	8.11	0.15	49.02	0.30	0.13	0.05	0.03	0.09	0.16	0.08	98.84
Cpx	40.04	2.68	10.35	10.86	0.17	8.94	22.87	0.43	0.02	0.04	0.96	0.11	0.76	98.27
Phlog	46.17	1.40	12.88	13.77	0.14	8.07	2.81	1.23	5.76	0.46	0.83	0.12	0.20	93.97
Amf	39.02	2.76	13.09	13.28	0.23	10.94	12.55	1.85	0.87	0.04	0.53	0.13	0.88	96.20
P = 0.5 GPa, T = 1250°C, H₂O fluid														
L _{Sil}	59.28	0.53	14.47	1.27	0.09	0.23	4.91	2.90	2.07	0.68	0.40	0.07	1.17	88.17
L _{Sr}	12.24	0.84	2.73	0.62	0.06	0.69	35.72	1.22	0.53	36.6	5.75	0.09	1.02	99.17
Cal	0.43	0.10	0.21	0.62	0.48	0.14	52.53	0.29	0.12	0.72	0.04	0.00	0.12	55.81
Ol	40.25	0.09	0.24	9.85	0.26	48.69	0.16	0.16	0.07	0.03	0.24	0.46	0.10	100.58
Cpx	44.28	2.51	7.71	11.72	0.34	8.83	21.46	0.72	0.10	0.22	0.73	0.13	1.14	99.90
Phlog	46.84	2.58	11.63	9.23	0.13	12.92	2.74	1.81	6.51	1.59	0.36	0.13	0.45	97.23
Amf	52.17	1.67	11.60	8.92	0.40	4.48	14.40	1.98	1.18	0.80	0.42	0.14	1.42	99.59
P = 0.5 GPa, T = 1250°C, H₂O+CO₂ fluid														
L _{Sil}	53.76	1.68	12.94	4.11	0.15	2.42	11.52	2.76	1.47	1.45	0.92	0.18	1.50	94.83
L _{Sr}	30.88	0.44	8.26	1.23	0.15	0.82	23.24	2.00	1.26	22.3	2.57	0.12	1.13	94.45
Ol	40.67	0.67	1.03	12.44	0.29	44.30	1.25	0.29	0.15	0.39	0.77	0.36	0.32	102.95
Cpx	45.66	2.53	8.51	9.81	0.21	10.76	19.76	0.86	0.35	0.59	0.77	0.13	1.04	100.97
Phlog	46.98	1.66	9.71	5.06	0.10	19.07	1.46	1.82	4.60	0.66	0.16	0.24	0.36	91.85
Amf	45.82	2.25	5.98	12.31	0.50	20.37	13.01	0.42	0.12	0.23	0.67	0.29	0.94	102.87
P=4 GPa, T=1250°C, «dry» system														
L _{Sil}	46.45	1.20	14.61	1.40	0.15	0.21	3.02	6.69	3.77	0.05	0.77	0.02	0.84	79.19
L _{Carb}	18.34	0.42	6.18	1.0	0.32	0.14	28.69	8.52	1.85	0.12	9.29	0.02	2.01	76.89
L _{Sulph}	0.15	0.06	0.1	45.11	0.10	0.02	0.19	0.05	0.07	52.0	0.24	0.12	-	98.27
Cpx	43.70	5.87	10.91	8.27	0.18	7.51	17.68	3.84	0.24	0.07	1.78	0.08	1.18	101.31
Phlog	38.42	4.74	15.43	9.74	0.18	16.90	1.56	1.13	9.77	0.12	0.62	0.17	0.49	99.28

Ol - olivine, *Cpx* - clinopyroxene, *Phlog* - phlogopite, *Amf* - amphibole, *L_{Sil}* - silicate melt, *L_{Sr}* - sulphate melt, *L_{Sulph}* - sulphide melt, *L_{Carb}* - carbonate melt, *Cal* - calcite.

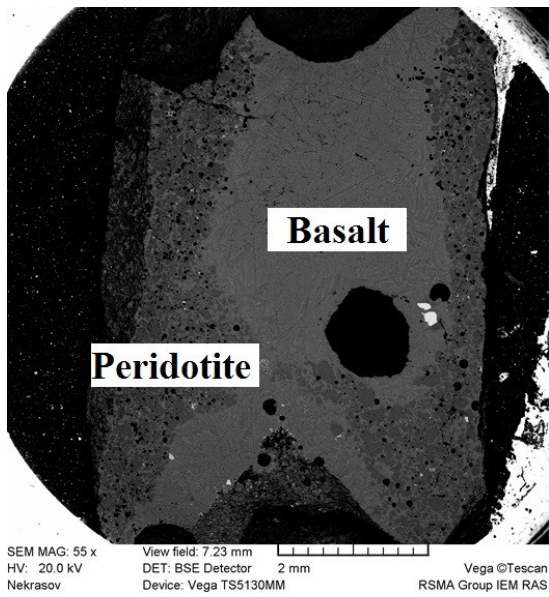
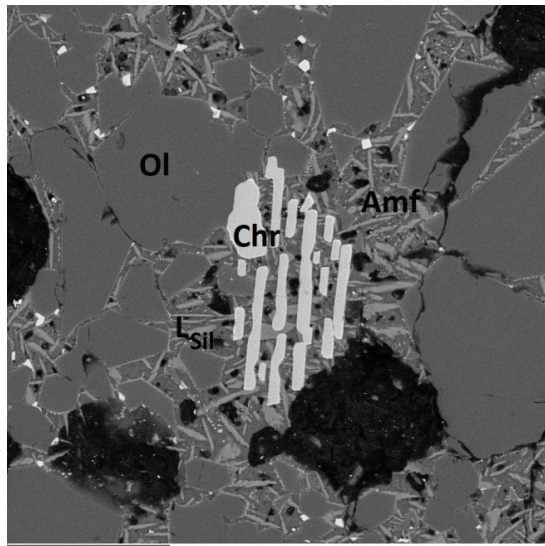
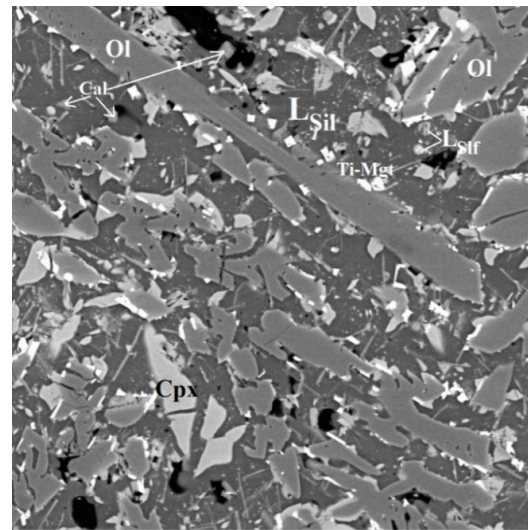


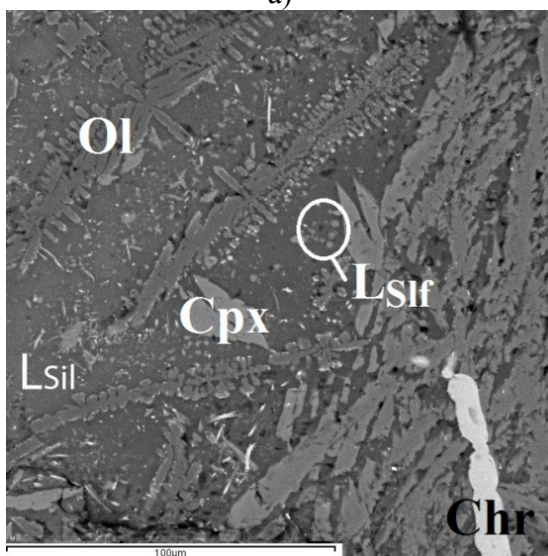
Fig. 1. BSE micrograph of a longitudinal section of the sample.



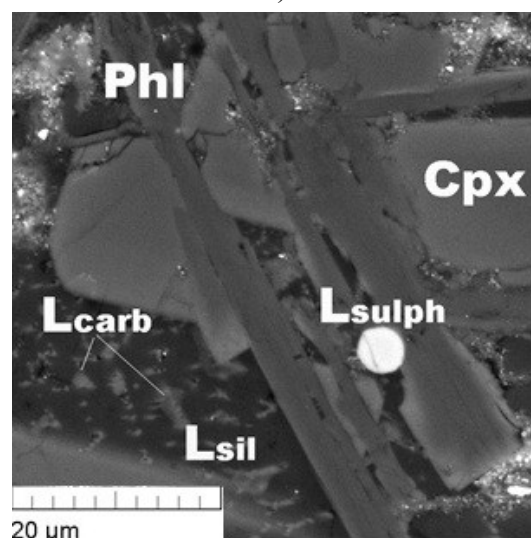
a)



b)



c)



d)

Fig. 2. BSE micrographs of polished samples after experiments. a) $T = 1250^{\circ}\text{C}$, $P = 0.3 \text{ GPa}$, H_2O fluid; b) $T = 1250^{\circ}\text{C}$, $P = 0.5 \text{ GPa}$, H_2O fluid; c) $T = 1250^{\circ}\text{C}$, $P = 0.5 \text{ GPa}$, $\text{H}_2\text{O} + \text{CO}_2$ fluid; d) $T = 1250^{\circ}\text{C}$, $P = 4.0 \text{ GPa}$, "dry" system.

Brief description of the experimental samples:

System of peridotite - basalt - (K, Na)₂CO₃ - H₂O fluid, T = 1250°C, P = 0.3 GPa. Silicate melt of andesite-basalt composition (SiO₂ - 53 wt.%) of normal alkalinity (K₂O + Na₂O ~ 4 wt.%) coexists with the association of Ol-Cpx-Amf-Phlog and accessory minerals - Chr, Ti-Mgt, Zrn (Fig. 2a).

System of peridotite - basalt - (K, Na)₂CO₃ - H₂O fluid, T = 1100°C, P = 0.5 GPa. Silicate melt of basaltic composition (SiO₂ - 50 wt.%) of normal alkalinity (K₂O + Na₂O ~ 4 wt.%) coexists with the association of Ol-Cpx-Amf-Phlog and accessory minerals - Chr, Ti-Mgt, Zrn.

System of peridotite - basalt - (K, Na)₂CO₃ - H₂O fluid, T = 1250°C, P = 0.5 GPa. Silicate andesitic melt (SiO₂ - 59 wt.%) of normal alkalinity (K₂O + Na₂O ~ 5 wt.%) coexists with Ol, Cpx, Amf, Phlog; AM - Chr, Ti-Mgt, Zrn. Drop-like sulphate melt (L_{SIF}) of anhydrite (CaSO₄) composition and carbonate phase (Cal) of calcite composition are present in the system (Fig. 2b).

System of peridotite - basalt - (K, Na)₂CO₃ - H₂O+CO₂ fluid, T = 1250°C, P = 0.5 GPa. Silicate melt of andesite-basalt composition (SiO₂ - 54 wt.%) of normal alkalinity (K₂O + Na₂O ~ 4 wt.%) coexists with the association of Ol-Cpx-Amf-Phlog and accessory minerals - Chr, Ti-Mgt, Zrn. The inclusions of microglobules of sulphate melt (L_{SIF}) are present in silicate melt. The carbonate phase is absent (Fig. 2c).

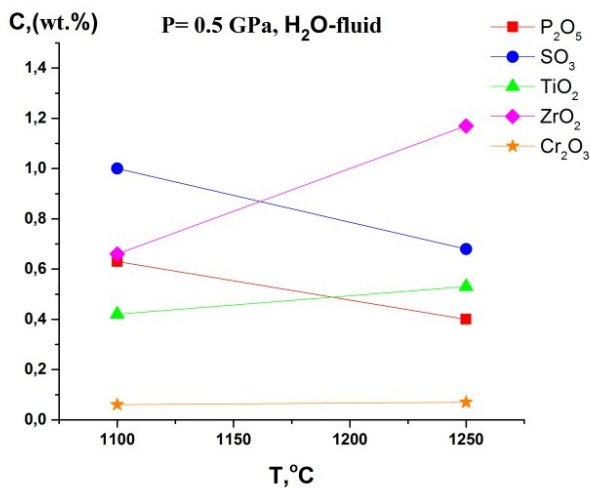
System of peridotite - basalt - (K, Na)₂CO₃, T = 1250°C, P = 4.0 GPa. Association of Cpx-Phlog + AM (Chr, Ti-Mgt, Zrn) cemented by intergranular silicate glass with inclusions of carbonate and

sulphide phases. The composition of the silicate melt is phonolites (SiO₂ - 54 wt.%, K₂O + Na₂O ~ 10-11 wt.%), composition of carbonate melt is significantly calcium with a mixture of alkali metal and silicate component (Fig. 2d).

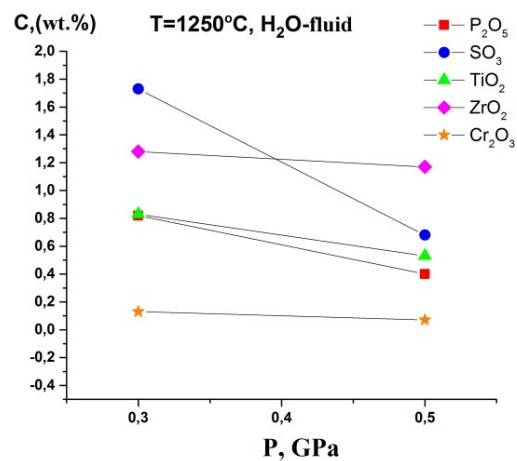
Solubility of accessory minerals. The indicator of solubility of AM were concentrations of P, S, Ti, Zr, Cr in silicate melts in equilibrium with their mineral concentrators (apatite, anhydrite or sulphide melt, Ti-magnetite, zircon, chromite). Content of P₂O₅, SO₃, TiO₂, ZrO₂, Cr₂O₃ in silicate melts are shown in Table 1.

At crust P (0.3-0.5 GPa) with increasing temperature from 1100 to 1250°C increases the concentration of ZrO₂ and TiO₂ in silicate melt. Concentration of SO₃ and P₂O₅ decreases (Table 1, Fig. 3a). With pressure increasing from 0.3 to 0.5 GPa, the solubility of all AM decreases (Table 1, Fig. 3b). The solubility of accessory minerals in H₂O+CO₂-containing melts higher than in H₂O-containing melts (Table 1, Fig. 3c).

Stratification of silicate melt into immiscible silicate, carbonate and sulphide melt was observed at mantle P = 4.0 GPa, T = 1250°C. Solubility of AM and concentration of typomorphic for them elements were identified only in coexisting carbonate and silicate melts. Distribution coefficients (K_D) of these elements were calculated between carbonate and silicate melts. K_D Zr, S, P, Na, Mn, Ca >1, consequently, these elements are concentrated mainly in the carbonate melt. Ti together with Si, Al, K, Mg, Fe are concentrated in the silicate melt, K_D < 1 (Fig. 3d).



a)



b)

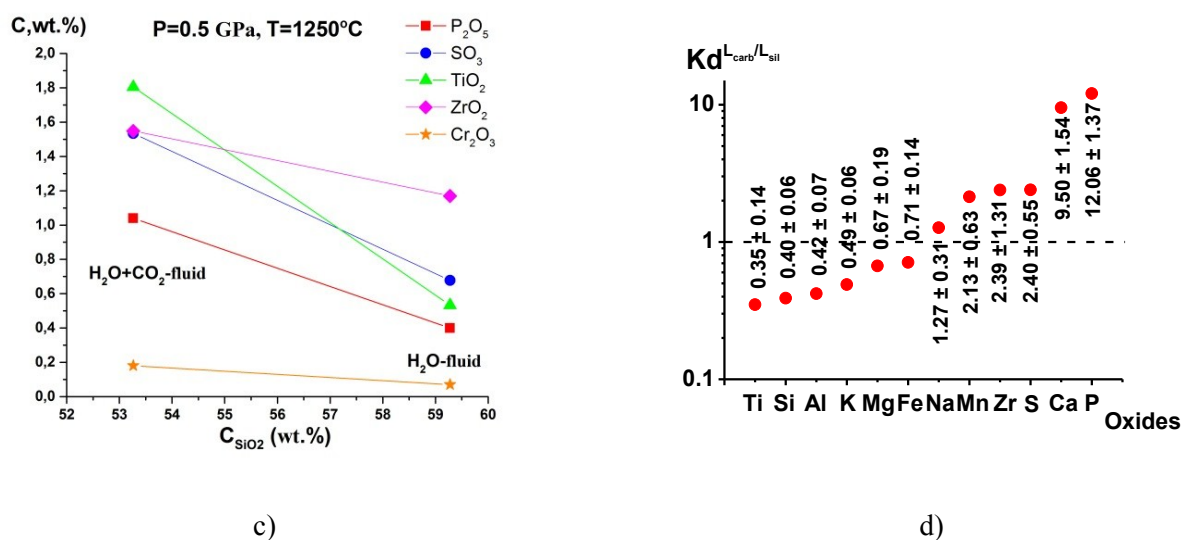


Fig. 3. Effect of temperature (a), pressure (b) and fluid composition, (c) on concentration of P₂O₅, SO₃, TiO₂, ZrO₂, Cr₂O₃ in silicate melts (at T = 1100-1250°C, P = 0.3-0.5 GPa). (d) - Distribution of major elements between coexisting silicate and carbonate melts (at T = 1250°C, P = 4.0 GPa).

Experimental study of the effect of T-P and fluid composition on the solubility of accessory minerals in silicate melts formed during partial melting of peridotite-basalt-(K, Na)₂CO₃ system at crust and mantle PT, showed:

- apatite was not detected in all experiments. This indicating high apatite solubility in melts. Thus, obtained P₂O₅ concentration in "dry" and fluid-containing silicate melts below the saturation concentration of melts by phosphorus at which apatite is stable. The saturation concentration of P₂O₅ in melts with H₂O+CO₂ fluid >1.0 wt.%, in water-containing melts >0.3 wt.% and > 0.8 wt.% in the "dry" melts;

- fluid composition influence on the melt compositions and solubility of AM. At P = 0.3-0.5 GPa in a water-containing system formed acidic melts from andesite to andesite-basalt; melts of basaltic composition formed in H₂O+CO₂-containing system. Under similar P-T solubility of AM in 2-3 times higher in H₂O+CO₂-containing melts than in H₂O-containing melts;

- at P = 0.3-0.5 GPa sulphur associated only with sulphate melt of anhydrite composition. High concentrations of sulphur in the melt (~ 1.5 wt.%) can be explained by the fact that the buffer CoCoO oxidation of sulphide sulphur (S²⁻) to sulphate (SO₄²⁻). According to the available experimental data, the concentration of sulphur in the water-containing melts in equilibrium with the sulphide melt at P ≤ 0.5 GPa are 0.1-0.2 wt.% [Kostyuk, Gorbachev, 2011; Kostyuk, Gorbachev, 2013], and in equilibrium with the sulphate melt - more than 1 wt.% [Jugo et al., 2005];

- stratification of silicate melt into immiscible silicate, carbonate and sulphide melt was observed at P = 4.0 GPa. The distribution coefficients of the main elements (including titanium, zirconium, phosphorus,

sulphur) between coexisting silicate and carbonate melt showed that the main concentrator of Na, Mn, Zr, S, Ca, P is carbonate melt; Si, Al, K, Mg, Fe, Ti - silicate melt.

This work was supported by RFBR grant №14-05-00752a.

References:

1. Litvin Y.A. (1991). Physic-chemical studies of the deep melting of the Earth. M. Science.
2. Gorbachev N.S. (1990). Fluid-magma interaction in sulfide-silicate systems. *Intern Geology Review*. V.32, N.8, P. 749-831
3. Jugo P.J., Luth R.W. and Richards J.P. (2005). An experimental study of the sulfur content in Basaltic melts saturated with immiscible sulfide or sulfate liquids at 1300°C and 1GPa. *Journal of Petrology*, V.46, N.4, P.783-798
4. Kostyuk A.V., Gorbachev N.S. (2011). The extreme pressure dependence of the solubility of sulfur in silicate melts (experimental data). *Electronic Scientific Information Journal "Vestnik of the Department of Earth Sciences RAS"* 3, NZ6045, doi: 10.2205/2011NZ000175
5. Kostyuk A.V., N.S. Gorbachev (2013). Is there an extreme pressure dependence of sulphur solubility in hydrous silicate melts? *Mineralogical Magazine*, July 2013, v. 77, p. 1414-1534, published online August 7, 2013, doi: 10.1180 / minmag.2013.077.5.11